Chapter 4

Pruned horseshoes

We will here discuss pruned horseshoe maps in two dimensions and we are going to discuss the ordering of bifurcations in these systems. We are not going to give a precise definition of this class of maps, but we believe this class includes many systems of interest in physics. Our motivation is the Hénon map, discussed in an enormous number of articles [3, 4, 22, 26, 27, 41, 45, 53, 92, 93, 107, 112, 150, 153, 180]. In particular we develop further the approach initiated by the work of Cvitanović, Gunaratne and Procaccia [53]. The complicated bifurcation structure in the parameter space (a, b) of the Hénon map has been noticed in several works [153, 150] and the most complete investigations on the bifurcation has been done by Mira and coworkers [75, 76, 77, 153]. The book by Mira, ref. [153], gives an impressing amount of numerical results but the discussion in the book is difficult to follow and Mira does not use the same notation as most other authors use. We claim that the methods we use apply to all maps "similar" to the Hénon map, and we give some examples of a perturbation of the Hénon map and of other maps for which the method works.

By an n-folding map we understand a map similar to a n-folding Smale horseshoe map which may be perturbed in such a way that its non-wandering set is not a full hyperbolic $n \times n$-Cantor set in the phase space. Under one iteration the perturbed horseshoe map should not fold any region of the phase space more than n times. The simplest folding maps are the once-folding maps, of which the Hénon map is the most well known. We may regard an n-folding map as the two-dimensional analogue of the 1-dimensional n-modal map. The bifurcation that leads to loss of orbits has to be similar to the bifurcations we find in the Hénon map. This excludes the 3-disk system and other billiards that we discuss later, because in billiard systems the bifurcations are not naturally organized in the same hierarchical structure.

We will construct here the bifurcation diagrams for the once-folding maps, and

we will also describe how we can extend this description of the once-folding map to the n-folding maps, and give an example for the 3-folding map. This is an analogue to our discussion of generalizing the unimodal method to n-modal 1-dimensional maps.

To be able to discuss a pruned horseshoe map in symbolic dynamics language we have to assume the following:

Conjecture: *An incomplete horseshoe can be described by a subset of the symbolic dynamics of the corresponding complete Smale horseshoe map.*

This conjecture works for all the examples we discuss, and we do not know any examples of once-folding systems that contradict it. An orbit may change symbols when a parameter changes but this is a consequence of bifurcations and does not contradict the conjecture. We will state below a conjecture on how to obtain a unique symbolic dynamics given the pruned horseshoe map.

The horseshoes in figures 3.1 and 3.7 can be realized by the Hénon map

$$\begin{aligned} x_{t+1} &= 1 - ax_t^2 + y_t \\ y_{t+1} &= bx_t \end{aligned} \tag{4.1}$$

or equivalent

$$x_{t+1} = 1 - ax_t^2 + bx_{t-1} \tag{4.2}$$

A non-smooth tent map version of this is the Lozi map:

$$\begin{aligned} x_{t+1} &= \begin{cases} 1 + ax_t + y_t & \text{if } x < 0 \\ 1 - ax_t + y_t & \text{if } x \geq 0 \end{cases} \\ y_{t+1} &= bx_t \end{aligned} \tag{4.3}$$

Grassberger and Kantz [92] have conjectured that the Hénon map may be described by binary symbols constructed by finding the primary homoclinic tangencies and use these to separate the nonwandering set into two regions denoted by the two symbols. Cvitanović, Gunaratne and Procaccia [53] have used such binary symbols to construct a "pruning front".

A different approach has been done by Biham and Wenzel, who constructed an algorithm that should always find a periodic orbit given a symbol string [26, 27]. This method starts with a guess for n values $\tilde{x}_0, \tilde{x}_1, \ldots, \tilde{x}_{n-1}$ of a given period n orbit. If this was a solution we would have $\Delta_t = \tilde{x}_{t+1} - (1 - a\tilde{x}_t^2 + b\tilde{x}_{t-1}) = 0$, with $0 \leq t \leq n-1$ and $\tilde{x}_0 = \tilde{x}_n, \tilde{x}_{-1} = \tilde{x}_{n-1}$. The nonvanishing errors $\Delta_t \neq 0$ in the general case can be used to change the numbers $\tilde{x}_t$ by the artificial dynamics

$$\frac{d\tilde{x}_t}{d\tau} = s_t \Delta_t \tag{4.4}$$

where $s_t \in \{-1, 1\}$ is the symbolic description of an orbit. This method converges to a period n orbit for most parameter values and symbol strings. We will discuss in section 4.5 why the method cannot always converge. At the moment we just accept the numerical fact that this method often converges, and gives one possible symbolic description of most periodic orbits.

We believe Grassberger-Kantz's point of view that it is possible to find primary homoclinic tangencies and to use these tangencies as the separation points between different symbols in the same way as we used critical points to define symbols in the 1-dimensional maps. Grassberger and Kantz found that it was not one unique way to choose the primary tangencies and different choices gave different possible separations with the same topological entropy. We avoid this ambiguity by a conjecture stated in section 5.2.1 on how to always have a unique set of primary tangencies which are connected by a continuous partition line.

4.1 Bifurcations

4.1.1 Stable and unstable manifolds at bifurcation points

To describe the bifurcations we have to investigate the manifolds of the map. When discussing bifurcations in 2-dimensional maps, pictures of the type in figure 4.1 are usually drawn. These pictures illustrate a homoclinic tangency bifurcation and are used when proving the results of Gavrilov and Silikov [84] and of Newhouse [160], see ref. [100]. In figure 4.1 b) the unstable and the stable manifolds are tangent at a point a finite distance from the hyperbolic point measured along the manifolds. This is a bifurcation analogue to the 1-dimensional map bifurcation where the critical point maps into the fixed point or into an unstable periodic orbit. In 1-dimensional maps this may be a band merging bifurcation, a crisis bifurcation or a chaotic attractor. This bifurcation where the unstable and the stable manifolds are tangent to each other is not the analogous case of the 1-dimensional tangent bifurcation creating a periodic orbit, but there is a bifurcation creating a periodic orbit arbitrarily close to the bifurcation in figure 4.1 b). The picture to draw studying this bifurcation is the drawing in figure 4.2.

In figure 4.2 a) the unstable manifold becomes folded and the turning point converges to a point in a periodic orbit. The stable manifold of a hyperbolic point does not get arbitrarily close to the periodic orbit at a finite distance from the hyperbolic point measured along the manifold. We are therefore not especially interested in the stable manifold when studying the bifurcation creating a stable periodic orbit. A useful drawing is figure 4.2 b) where we have plotted the unstable

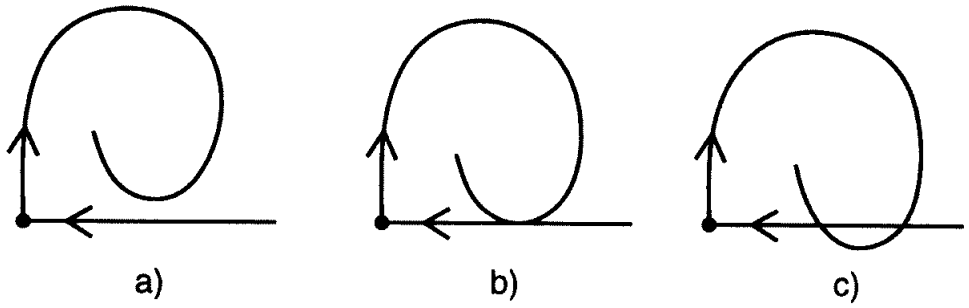

Figure 4.1: A bifurcation where the stable and unstable manifold create a homoclinic point.

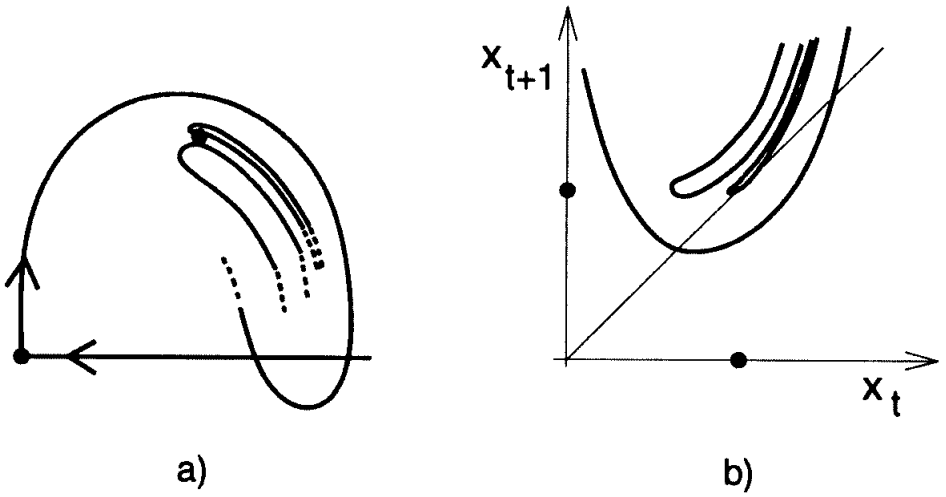

Figure 4.2: a) The two manifolds close to a bifurcation creating a period n orbit. b) The n-th return map of the unstable manifold close to a bifurcation creating a period n orbit.

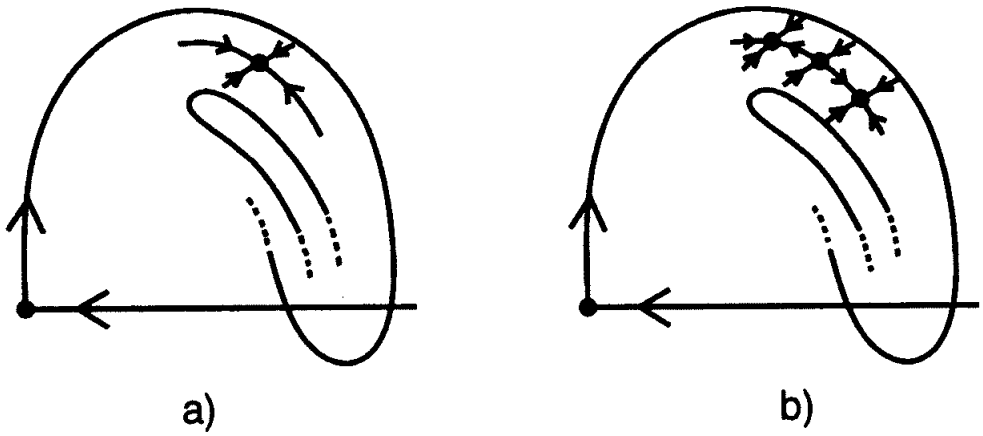

Figure 4.3: The period doubling bifurcation of a periodic orbit.

manifold in the space (x_t, x_{t+n}) where n is the length of the periodic orbit created at the bifurcation. In this space the unstable manifold converges to a curve which is tangent to the diagonal $x_{t+n} = x_t$. The bifurcation is therefore well described by a 1-dimensional map of the unstable manifold.

The period doubling bifurcation is illustrated in figure 4.3. This is a local bifurcation of the periodic orbit and no information of this bifurcation can be obtained by the stable manifold of the hyperbolic point. This stable manifold is never close to the periodic orbit bifurcating inside the basin of attraction. The periodic doubling bifurcation can also be studied by a 1-dimensional map of the unstable manifold.

To be able to apply the symbolic description we use the union of the unstable and stable manifolds for all points in the non-wandering set. We include the manifolds of all hyperbolic orbits, also of an orbit just having a period doubling bifurcation as in figure 4.3 b).

The homoclinic tangency in figure 4.1 b) is the point when the unstable manifold "turns back". We define a *turning point* or a *turnback* to be a point on the unstable manifold where the closest fold of the stable manifold is parallel to the unstable manifold. By this definition we have a turning point in all the three figures 4.1 a) 4.1 b) 4.1 c), but only in figures 4.1 b) do we know that we have a homoclinic tangency. If there is a homoclinic tangency in the other figures this point is identical to the turning point. A turning point may be inside the basin of attraction of a stable periodic orbit. We also use the term turnback for the non-smooth map like the Lozi-map for a point on the unstable manifold where the unstable manifold has a kink.

The turnbacks in the horseshoe maps play the same role as the critical points

in a 1-dimensional map when we study the bifurcations of the map.

There is always at least one turnback close to a stable orbit. The folds of the unstable manifold have a Cantor set structure and each fold has a turnback which can give a stable periodic orbit. This imply that the parameter space is infinite and we can obtain a map with any number of stable orbits existing simultaneously [160]. The bifurcations take place in an infinite dimensional parameter space which seems to be a hopeless system to describe. There are however two observations that simplify the bifurcation description. First; if a turning point gives a stable periodic orbit then the basin of attraction covers all the turnbacks in a neighborhood reducing other possible bifurcations close to this. Second; for the horseshoes there is a natural ordering or hierarchical organization of the folds allowing a systematic approximation scheme of the infinite dimensional parameter space. This is not true for all systems, e.g. billiard systems can not be described in this way.

4.1.2 One-dimensional approximation

The first approximation we make is to consider the horseshoe with n folds to be an n-modal 1-dimensional map $x_t = f(x_{t+1})$ with n parameters. The topological structure of the bifurcations can be described by the kneading sequences of the critical points (turning points) and we can draw a symbolic parameter space. The bifurcation diagrams are given in chapter 1. This unimodal description of the system is a necessary starting point, but not a remarkable result. In a realization of the pruned once-folding horseshoe e.g. the Hénon map, the unimodal bifurcations are not enough to explain the main features of the bifurcation curves in a parameter plane, (a, b), scan. One way to illustrate this approximation is to regard the image obtained by the Smale horseshoe map $g(Q)$ as a line instead of a band. The line is then a 1-dimensional function with a slope depending on the orientation of Q_k. This is equivalent to squeezing all the folds in the unstable manifold together to one curve. This is realized in the Hénon map in the limit $b \to 0$.

The second approximation is obtained by finding the second iterated of the horseshoe map, $g^2(Q)$, and make a 1-dimensional map where the intersections $g^2(Q) \cap Q$ correspond to monotone sections in a 1-dimensional map. If we look at the once-folding map in figures 3.3 and 3.8 we see that if we approximate the band $g^2(Q)$ with a curve this gives a trimodal map with two maximum and one minimum point. The minimum point is however the image of the bending point of $g(Q)$ and is not an independent critical point. This gives a two parameter map with two maximum points as the critical points of interest. The natural choice of the 1-dimensional map is a combination of two unimodal map with two critical points

x_c^0 and x_c^1 where both are maximum points. The kneading sequences from these two critical points give the two dimensional symbolic parameter space. The minimum point has as its only function that if it is as high as one of the maximum points the number of critical points decreases in the way we have discussed for trimodal maps in section 2.2. This kind of bifurcation makes it possible for an orbit in the two dimensional map to change symbolic description without getting stable by moving around a cusp as illustrated in the trimodal 1-dimensional map. The height of the minimum point described in symbols is found by a shift in the kneading sequence of x_c^0 or x_c^1. We then get two values for the minimum point and we have to be careful when discussing this minimum point.

The third approximation is obtained by simplifying $g^{(3)}(Q)$ by choosing a line for each intersection $g^{(3)}(Q) \cap Q$. For the once-folding map in figures 3.4 and 3.9 we get a 7 modal map with 4 independent critical points and we can describe this by four unimodal maps. Again only the kneading sequence of the maximum points are critical points of interest in the once-folding horseshoe. The minimum points are images of the maximum points in the first and second approximation. The parameter space is four dimensional, and we construct the topological parameter space from the kneading sequences of the four critical points x_c^{00}, x_c^{01}, x_c^{10} and x_c^{11}.

The n-th approximation of the once-folding map is now obtained by considering $g^{(n)}(Q)$ to be a 1-dimensional map consisting of 2^{n-1} unimodal maps. The 2^{n-1} maximum points $x_c^{0\ldots00}$, $x_c^{0\ldots01}$, $x_c^{0\ldots10}$, $\ldots$, $x_c^{1\ldots11}$ are the critical points of interest and the kneading sequence of these points give the topological parameter space. The maximum points correspond to the primary turnbacks, while the minimum points correspond to turnbacks that are not primary.

The two-folding map in figure 3.15 is approximated the same way. The first approximation gives a bimodal map with a maximum point x_{c1} and a minimum point x_{c2} and the bifurcation diagrams discussed in section 1.1. The second approximation gives two bimodal maps with the six critical points x_{c1}^0, x_{c1}^1, x_{c1}^2, x_{c2}^0 x_{c2}^1 and x_{c2}^2. The other extremum points are images of the extremum points in the first approximation and corresponds to turnbacks that are not primary. The n-th approximation gives $\cdot 3^{n-1}$ bimodal maps with $2 \cdot 3^{n-1}$ independent critical points, and a $2 \cdot 3^{n-1}$ dimensional parameter space.

A m-folding map have in the n-th approximation $m \cdot (m+1)^{n-1}$ independent critical points, and a $m \cdot (m+1)^{n-1}$ dimensional parameter space.

4.2 Unimodal approximation

The first approximation gives exactly the MSS ordering of periodic orbits as we have discussed in chapter 1 for the once-folding map. This is the ordering we find for the Hénon map and the Lozi map in the limit $b \to 0$.

4.3 Bimodal approximation

The second approximation gives a bimodal map with a two dimensional parameter plane. The topological parameter plane is different from the bimodal three-symbol plane discussed in section 2.1, and we can describe this topological bifurcation plane by using the restrictions we find on the binary symbols.

The two unimodal maps $f_0(x_t)$ and $f_1(x_t)$ corresponds to the two folds in $g^{(2)}(Q)$ and each fold is the image of one of the two parts of $g(Q) \cap Q$; Q_0 and Q_1. From the figures 3.1 and 3.3 we find that for the Smale horseshoe without any reflection Q_0 maps into the outer fold and Q_1 maps into the inner fold. The drawings of the Smale horseshoe with reflections, figures 3.6 and 3.8, show that in this case Q_0 maps into the inner fold and Q_1 maps into the outer fold. The inner fold has a maximum point that are smaller than the maximum point of the outer fold which imply; for not reflected maps $x_c^1 < x_c^0$, and for reflected maps $x_c^0 < x_c^1$. The function of the 1-dimensional map applied to a point x_t is $f_0(x_t)$ if x_{t-1} is in Q_0 which is equivalent to that $s_{t-1} = 0$. The function applied to the point x_t is $f_1(x_t)$ if x_{t-1} is in Q_1 that is if $s_{t-1} = 1$.

The bimodal map is

$$x_{t+1} = f_{s_{t-1}}(x_t) \tag{4.5}$$

We can now find all periodic orbits of a given length and find the topological values $\tau_s(\overline{S})$ of all cyclic permutations of the orbits.

4.3.1 Kneading values of short orbits

The fixed point $\overline{0}$ has $s_{-1} = 0$ and the only kneading value is $\tau_0(\overline{0}) = 0$. This orbit exists when

$$\kappa_0 > \tau_0^{\max}(\overline{0}) \;\; = \;\; 0 \tag{4.6}$$

The fixed point $\overline{1}$ has $s_{-1} = 1$ and kneading value is $\tau_1(\overline{1}) = 0.\overline{10} = 2/3$ and it exists for symbolic parameter values

$$\kappa_1 > \tau_1^{\max}(\overline{1}) \;\; = \;\; 0.\overline{10} = 2/3 \tag{4.7}$$

The period 2 orbit $\overline{10}$ has two cyclic permutations. The point x_{10} with symbolic description $\overline{s_1 s_2} = \overline{10}$ has $s_0 = s_2 = 0$ and $s_{-1} = s_1 = 1$ giving the kneading value $\tau_1(\overline{10}) = 0.\overline{1100} = 4/5$. The second point in the period 2 orbit, x_{01}, is on map 0 since $s_{-1} = 0$ and the kneading value is $\tau_0(\overline{01}) = 0.\overline{0110} = 2/5$. This orbit exists for the symbolic parameter values

$$\kappa_0 > \tau_0^{\max}(\overline{10}) = 0.\overline{0110} = 2/5 \tag{4.8}$$
$$\kappa_1 > \tau_1^{\max}(\overline{10}) = 0.\overline{1100} = 4/5 \tag{4.9}$$

There are two period 3 orbits with the symbolic strings $\overline{s_1 s_2 s_3}$: $\overline{100}$ and $\overline{101}$. Here we have that $s_{-1} = s_2$ describes which map the point is on. The orbit $\overline{100}$ has the following symbolic values: $\tau_0(\overline{100}) = 0.\overline{111000} = 8/9$, $\tau_1(\overline{010}) = 0.\overline{011100} = 4/9$, $\tau_0(\overline{001}) = 0.\overline{001110} = 2/9$. The two values of interest are $\tau_0^{\max}(\overline{100}) = 8/9$ and $\tau_1^{\max}(\overline{100}) = 4/9$. The symbolic parameters where $= \overline{100}$ exists is

$$\kappa_0 > \tau_0^{\max}(\overline{100}) = 0.\overline{111000} = 8/9 \tag{4.10}$$
$$\kappa_1 > \tau_1^{\max}(\overline{100}) = 0.\overline{011100} = 4/9 \tag{4.11}$$

The second orbit has the three symbolic values: $\tau_0(\overline{101}) = 0.\overline{110} = 6/7$, $\tau_1(\overline{110}) = 0.\overline{100} = 4/7$, $\tau_1(\overline{011}) = 0.\overline{010} = 2/7$, and the orbit exists for symbolic parameter values

$$\kappa_0 > \tau_0^{\max}(\overline{101}) = 0.\overline{110} = 6/7 \tag{4.12}$$
$$\kappa_1 > \tau_1^{\max}(\overline{101}) = 0.\overline{100} = 4/7 \tag{4.13}$$

There are three period 4 orbits $\overline{1000}$, $\overline{1001}$ and $\overline{1011}$. The maximum kneading values and the symbolic parameter values where these orbits exist are

$$\kappa_0 > \tau_0^{\max}(\overline{1000}) = 0.\overline{11110000} = 16/17 \tag{4.14}$$
$$\kappa_1 > \tau_1^{\max}(\overline{1000}) = 0.\overline{00111100} = 4/17 \tag{4.15}$$
$$\kappa_0 > \tau_0^{\max}(\overline{1001}) = 0.\overline{1110} = 14/15 \tag{4.16}$$
$$\kappa_1 > \tau_1^{\max}(\overline{1001}) = 0.\overline{0100} = 4/15 \tag{4.17}$$
$$\kappa_0 > \tau_0^{\max}(\overline{1011}) = 0.\overline{10010110} = 10/17 \tag{4.18}$$
$$\kappa_1 > \tau_1^{\max}(\overline{1011}) = 0.\overline{11010010} = 14/17. \tag{4.19}$$

All these orbits of length 1, 2, 3 and 4 are drawn in figure 4.4. Here we see which of the two maps the points in the orbit lies on.

The curves for these bifurcations in the topological parameter plane is drawn in figure 4.5. This figure gives the description of a parameter space assuming that only the bimodal approximation is important and that the map has two maximum points.

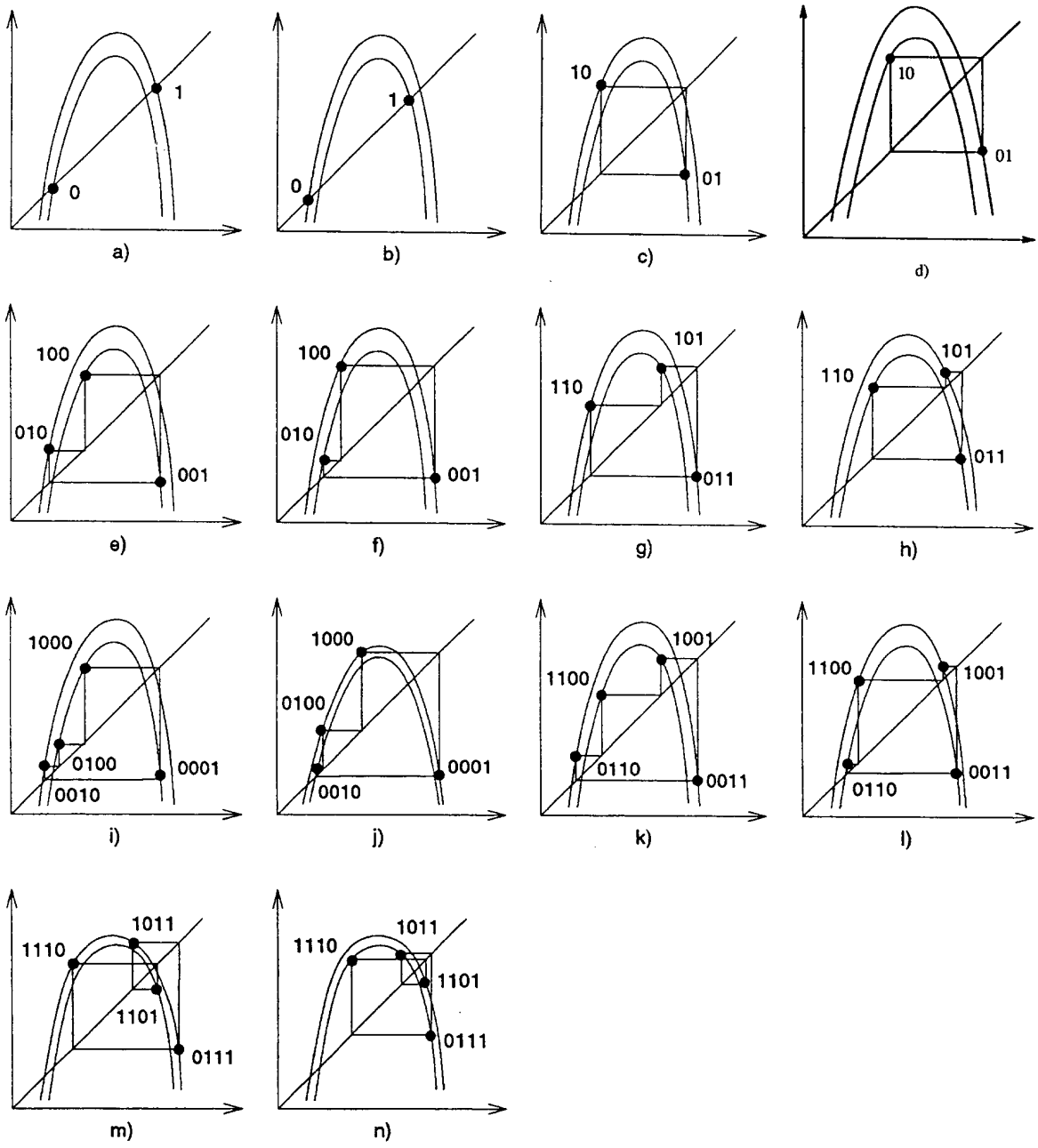

Figure 4.4: The the periodic orbits of length 1, 2, 3 and 4 in the bimodal approximation for the once-folding map. a), c), e), g), i), k) and m) shows once-folding maps with reflection ($b > 0$), the others without reflection ($b < 0$).

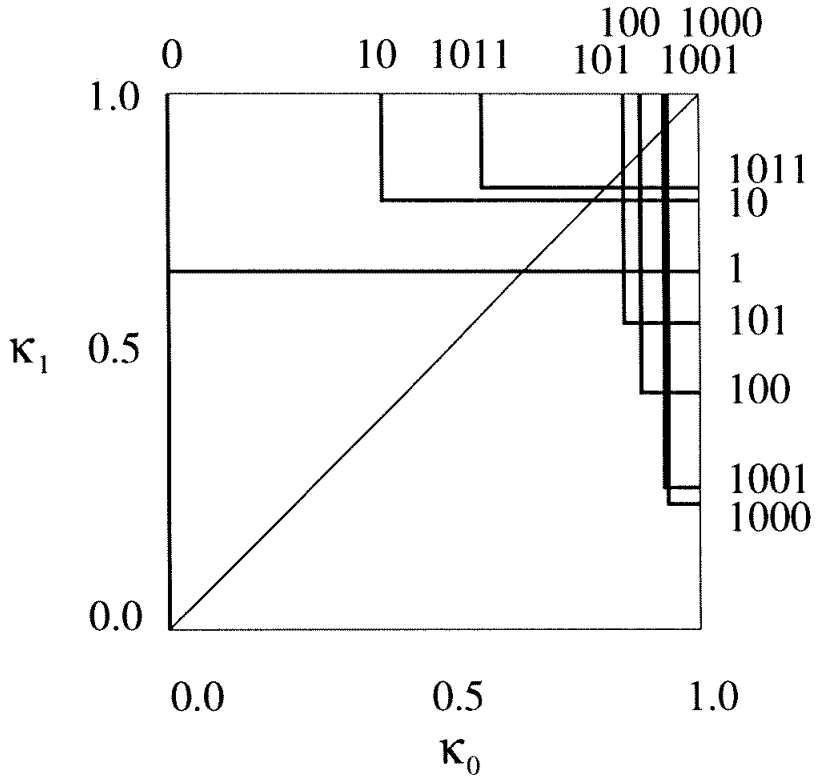

Figure 4.5: The bifurcations of the periodic orbits of length 1, 2, 3 and 4 in the topological parameter space of the bimodal approximation for the once-folding map.

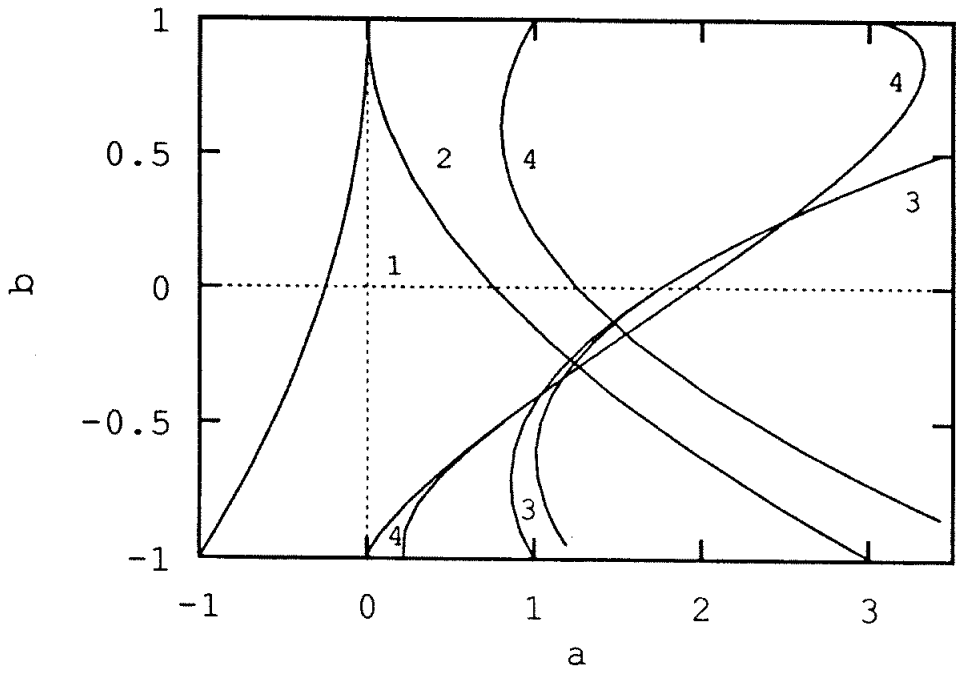

Figure 4.6: The bifurcation curves of the stable periodic orbits with period 1, 2, 3 and 4 in the parameter space of the Hénon map.

This figure can be compared with a two parameter scan of different once-folding maps. The relation between the topological parameter space (κ_0, κ_1) and a real parameter space (a, b) is as for the 1-dimensional maps: The structure of bifurcation curves is the same for the two spaces, but metric properties like smoothness and scaling are different. Figure 4.6 shows the areas in the (a, b) plane for the Hénon map where the periodic orbits of period 1, 2, 3 and 4 are stable. When comparing the drawings we should remember that the diagonal $\kappa_0 = \kappa_1$ corresponds to $b = 0$ in the Hénon map, a positive parameter value b to the triangle $\kappa_0 < \kappa_1$ which is the horseshoe with reflection, and a negative parameter value b corresponds the triangle $\kappa_0 > \kappa_1$ which is the horseshoe map without a reflection. The corner $\kappa_0 = \kappa_1 = 1.0$ in the topological parameter plane corresponds to the complete Smale horseshoe which is realized by the Hénon map for $b = 0$ with $a \geq 2$ and and for $b \neq 0$ with a sufficiently large [153].

The structure in the two figures is similar. For $b < 0$ figure 4.6 shows that the bifurcation curves for the period 3 orbits crosses the period 2 orbit bifurcation curves. The bifurcation curves for the period 4 orbits $\overline{1000}$ and $\overline{1001}$ crosses both the bifurcation lines for the period 2 and the period 3 orbits. For $b > 0$ the bifurcation curves are similar but for the Hénon map the period 4 orbits $\overline{1000}$ and $\overline{1001}$ crosses

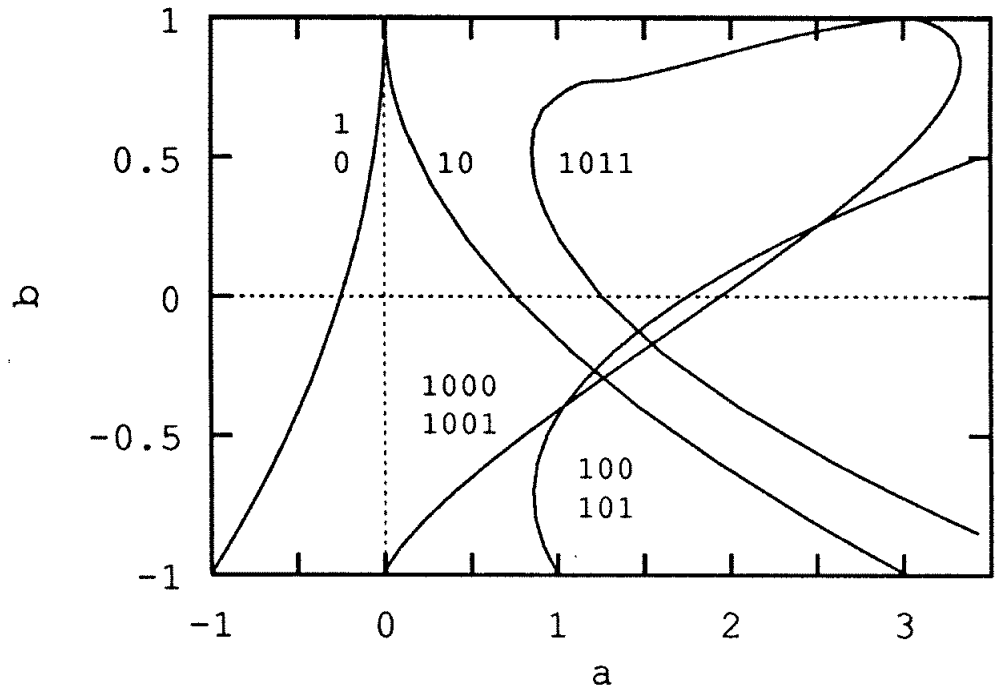

Figure 4.7: The bifurcation curves of the periodic orbits with period 1, 2, 3 and 4 in the parameter space of the Hénon map calculated by using the complex Biham-Wenzel method.

the period 3 curves for a larger value of a. This is not the case in figure 4.5. We show later that there is another bifurcation of the period 4 orbit that will be explained in the next order of approximation.

This is actually better than one could expect, because in drawing figure 4.5 we ignored the possibility that a maximum point of the 1-dimensional approximation could disappear in a bifurcation together with the minimum point. This bifurcation of critical points actually makes it impossible that the period 2 orbit $\overline{10}$ and the period 4 orbit $\overline{1011}$ bifurcate by decreasing κ_0 and that the orbits $\overline{100}$, $\overline{101}$, $\overline{1000}$ and $\overline{1001}$ bifurcate by decreasing κ_1.

The bifurcation of the critical points has taken place if the iteration of the maximum point gives a point larger than the minimum point. A periodic orbit can therefore not be pruned on map 0 (1) if the kneading value $\tau_0^{\max}$ ($\tau_1^{\max}$) is smaller than the kneading value of the once shifted symbol sequence. The value of the shifted sequence $\sigma(S)$ is larger than the value of the original sequence S if the value $\tau(S)$ is $\tau(\overline{0}) < \tau(S) < \tau(\overline{1})$:

$$0 < \tau_i^{\max}(S) <= 0.\overline{10} = 2/3 \tag{4.20}$$

From the kneading values of the period 2 orbit in eq. (4.8) and (4.9) we find that the orbit $\overline{10}$ only can be pruned by κ_1.

The period 3 orbits have kneading values given by eq. (4.10) – (4.13) and can only be pruned by κ_0 and not by κ_1.

The period 4 orbits $\overline{1000}$ and $\overline{1001}$ can as for the period 3 orbits only be pruned by κ_0, while the orbit $\overline{1011}$ is pruned by κ_1 but not by κ_0 as the orbit $\overline{10}$.

The exact description of the change from two to one maximum point in the 1-dimensional approximation is more complicated than the argument above. The following problem is a result of our approximation and is not present in the real horseshoe map: The two fold approximation have one minimum point which is the image of the maximum point of the one fold approximation. The problem in this statement is that we mix two different orders of approximation when we describe the minimum point. The symbolic description of the minimum point of the two fold approximation is then obtained by a shift operation on the maximum point of the one fold approximation. What we have used as the rule in eq. (4.20) is to use the shifted lower maximum point in the two fold approximation as the minimum point. This is a restrictive chose such that the topological description may forbid structures that exists in the horseshoe. This may explain qualitatively that the Hénon bifurcation plane in figure 4.6 shows similar structures as the topological parameter plane in figure 4.5 also for $\kappa_0 < 2/3$ and $\kappa_1 < 2/3$.

By using the method of Biham and Wenzel we can also find bifurcation lines for the orbits given their symbolic description. This diagram is given in figure 4.7. By comparing figure 4.7 and figure 4.6 we find that they are almost identical except that the bifurcation curve for $\overline{1011}$ in figure 4.7 close to $b = 1$ change direction and hit the bifurcation curves for $\overline{1000}$ and $\overline{1001}$ at $a = 3$, $b = 1$.

The bifurcations in the once-folding tent map (the Lozi map) (4.3) is drawn in figure 4.8. The bifurcation lines are a bit different than for the Hénon map, but the overall structure is as the topological parameter plane predicts. In the same way as the bifurcation curves for the Hénon map calculated by the Biham-Wenzel method, the period 4 orbits $\overline{1000}$ and $\overline{1001}$ for large positive b values get above the bifurcation lines of the period 3 orbits $\overline{100}$ and $\overline{101}$ and collide with the period 4 orbit $\overline{1011}$ line at $b = 1$. This we show later is a result of a trimodal bifurcation and is explained at the next level of approximation. A typical bifurcation in the Lozi map is that all period doublings take place at one parameter value as for the 1-dimensional tent map. One exception we find here is that for $b > 0$ the bifurcation lines for the orbits $\overline{10}$ and $\overline{1011}$ split, and therefore the period 2 orbit is stable in a triangle in the parameter plane in figure 4.8.

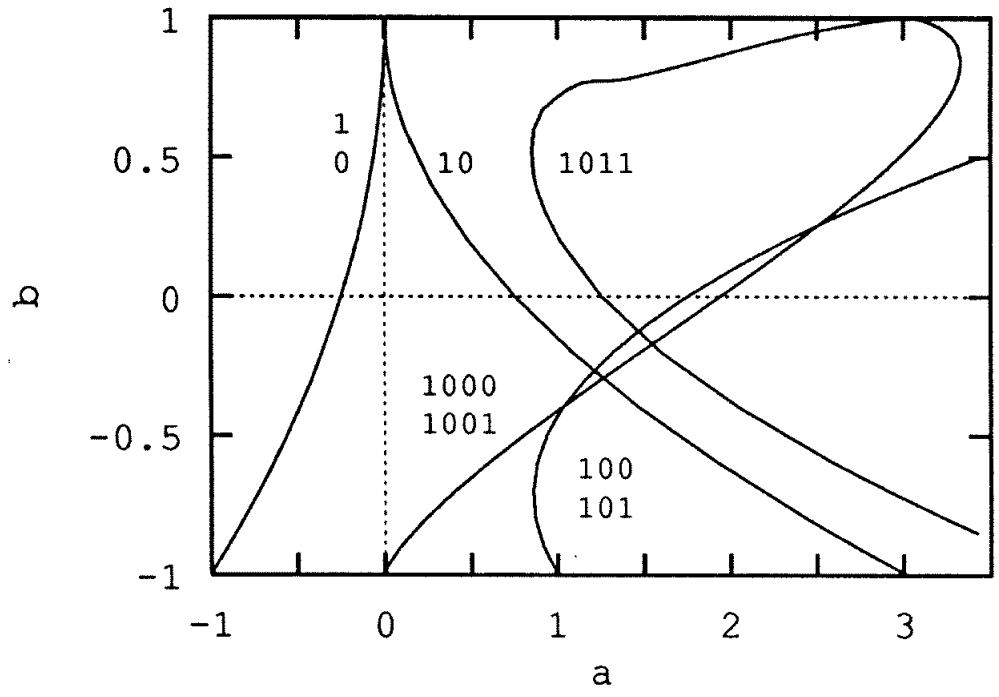

Figure 4.8: The bifurcations of the periodic orbits 1, 2, 3 and 4 in the parameter space of the Lozi map.

4.3.2 Period 5 orbits

The period 5 orbit gives the simplest example of the swallowtail cross in the bimodal approximation of the once-folding map. The six different period 5 orbits exist for the following topological parameter values:

$$\kappa_0 > \tau_0^{\max}(\overline{10000}) = 0.\overline{1111100000} \quad (4.21)$$
$$\kappa_1 > \tau_1^{\max}(\overline{10000}) = 0.\overline{0001111100} \quad (4.22)$$
$$\kappa_0 > \tau_0^{\max}(\overline{10001}) = 0.\overline{11110} \quad (4.23)$$
$$\kappa_1 > \tau_1^{\max}(\overline{10001}) = 0.\overline{00100} \quad (4.24)$$
$$\kappa_0 > \tau_0^{\max}(\overline{10011}) = 0.\overline{1011101000} \quad (4.25)$$
$$\kappa_1 > \tau_1^{\max}(\overline{10011}) = 0.\overline{1110100010} \quad (4.26)$$
$$\kappa_0 > \tau_0^{\max}(\overline{10010}) = 0.\overline{11000} \quad (4.27)$$
$$\kappa_1 > \tau_1^{\max}(\overline{10010}) = 0.\overline{11100} \quad (4.28)$$
$$\kappa_0 > \tau_0^{\max}(\overline{10110}) = 0.\overline{1100100110} \quad (4.29)$$
$$\kappa_1 > \tau_1^{\max}(\overline{10110}) = 0.\overline{1101100100} \quad (4.30)$$
$$\kappa_0 > \tau_0^{\max}(\overline{10111}) = 0.\overline{10110} \quad (4.31)$$
$$\kappa_1 > \tau_1^{\max}(\overline{10111}) = 0.\overline{11010}. \quad (4.32)$$

The bifurcation diagram is drawn in figures 4.9 and 4.10.

The first two orbits can not be pruned by κ_1 from the inequalities (4.22) and (4.24) because the critical point on map 1 disappear before one obtain the pruning value in the bimodal approximation. As for the period 3 orbits, a shift of the symbols gives a larger symbolic value.

The other four period 5 orbits can be pruned by both κ_0 and κ_1.

By choosing $\epsilon_i \in \{0, 1\}$ for $i = 1$ and $i = 2$ the string $\overline{10\epsilon_1 1\epsilon_2}$ gives the symbolic description of these four orbits which will have a bifurcation in a swallowtail cross. This is a bifurcation we know from the simple bimodal maps in section 2.1. Figure 4.10 shows the cross in the symbol plane where the gray area is the symbolic values that can not be obtained from kneading sequences of the critical points. This topological swallowtail cross can be compared with our numerical examples of the pruned horseshoe.

Figures 4.11 and 4.12 show the bifurcation lines of the Hénon map and the Lozi map. The area with stable period 5 orbits in figure 4.11 a) is the typical swallowtail with the same geometrical structure as in figures 2.4, 2.6 and 2.8. We expect the scaling of the period doubling of the crosses to be the same as for a bimodal one-dimensional map. MacKay and van Zeijts [142] showed that the swallowtail crossing

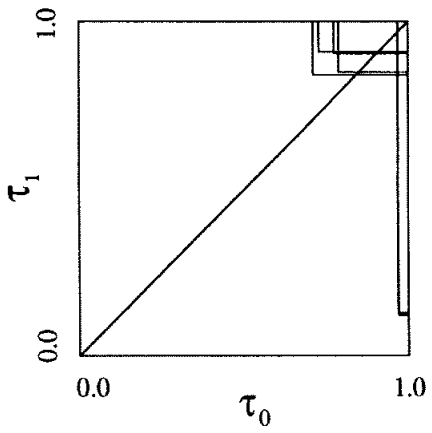

Figure 4.9: The bifurcation lines of all period 5 orbits in the symbol plane (κ_0, κ_1).

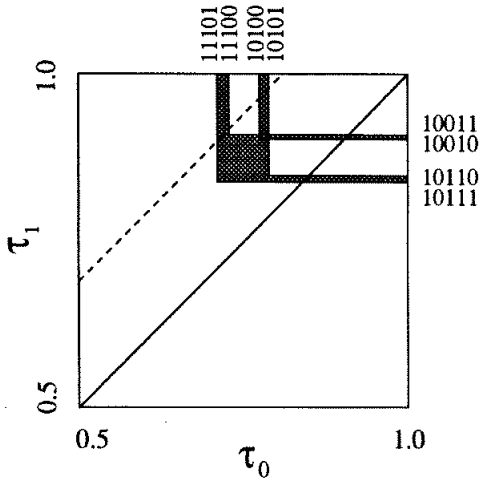

Figure 4.10: The bifurcation lines of the period 5 orbits giving a binary swallow tail in the symbol plane (κ_0, κ_1).

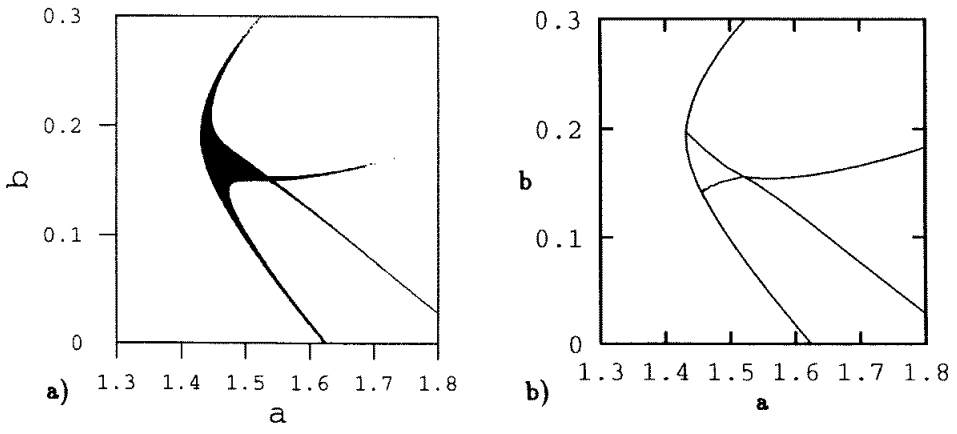

Figure 4.11: The swallowtail of period 5 orbits in the parameter plane (a, b) for the Hénon map. a) Areas with stable period 5 orbit. b) Bifurcation lines calculated with the complex Biham-Wenzel method.

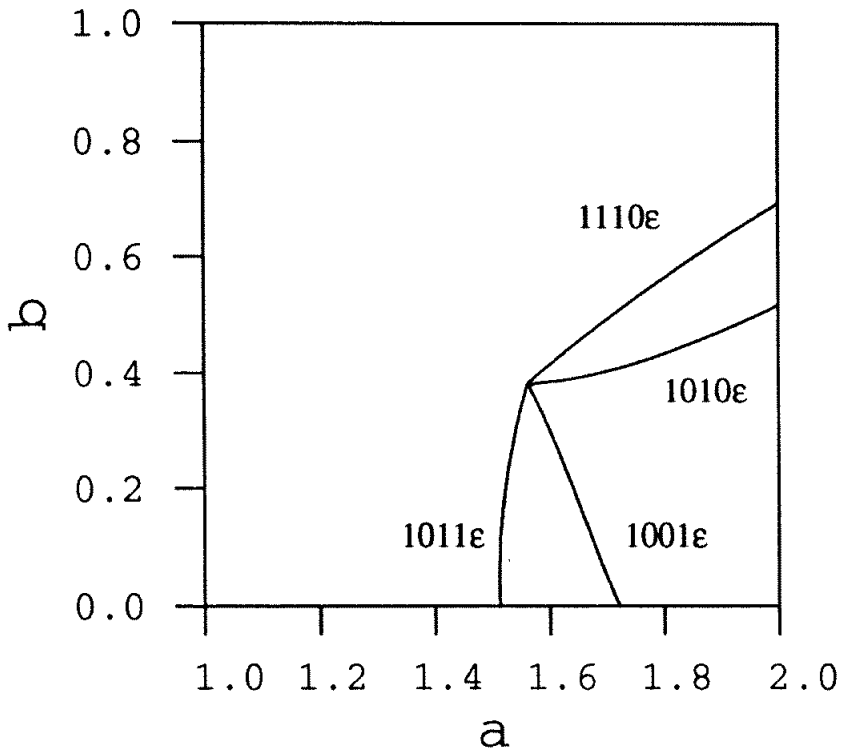

Figure 4.12: The swallowtail of period 5 orbits in the parameter plane (a, b) for the Lozi map.

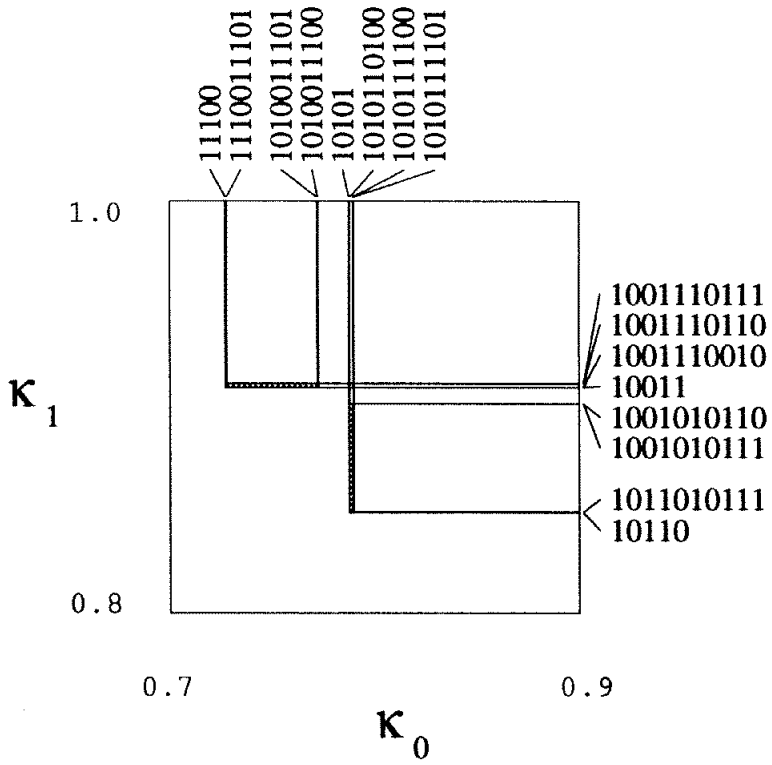

Figure 4.13: The bifurcation lines of period 10 orbits bifurcating from the period 5 swallowtail in the symbol plane (κ_0, κ_1).

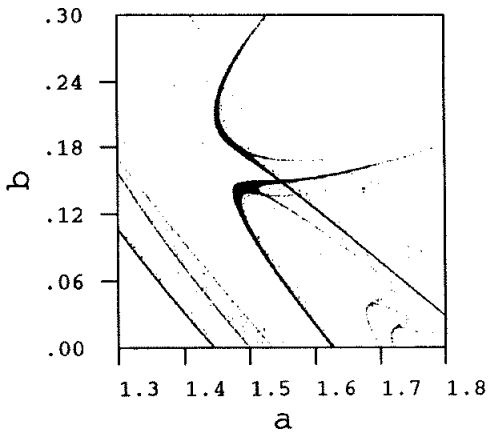

Figure 4.14: The period 10 orbits from the period doubling bifurcation of the period 5 orbits in the parameter plane (a, b) for the Hénon map.

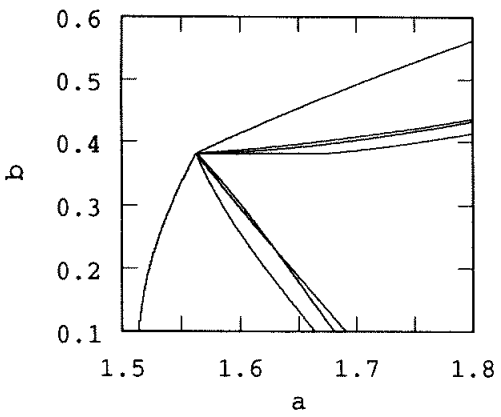

Figure 4.15: The period 10 orbits from the period doubling bifurcation of the period 5 orbits in the parameter plane (a, b) for the Lozi map.

scales with a spectrum of exponents, where the exponent changes with the path one follows in the renormalization of the parameter plane. Figure 4.14 shows the period 10 swallowtails from the period doubling of the period 5 swallowtail of the Hénon map.

The period 10 swallowtails are drawn in the symbolic parameter plane in figure 4.13. This is, using MSS terminology [147], the harmonics of the period 5 swallowtail orbits. The symbolic description is obtained by repeating twice the given cyclic permutation of the 5 symbols and change the last symbol. The scaling of crossings is different in this plane from the normal parameter plane.

Figure 4.11 b) shows the period 5 swallowtail crossing obtained by using the complex Biham Wenzel method. This method gives the tails and the crossing of the swallowtail. In the tails the method converges for both the stable and the unstable orbit up to practically the same bifurcation value. Inside the crossing however does the BW method not converge to the stable orbit. This is the region where a stable orbit in a one-dimensional map changes symbolic description in a rather complicated way sketched in figure 2.11 for the bimodal map. The BW method does not converge in this region while it converges without problems to the stable orbit in the tails where the symbols for an orbit in the one-dimensional map is more simple. The BW method finds here all the unstable orbits that exist.

The period 5 swallowtail crossing for the Lozi map in figure 4.12 is a crossing of bifurcation lines instead of a window structure in the (a, b) plane. Apart from this, the structure is the same as for the Hénon map. The crossing and all the period

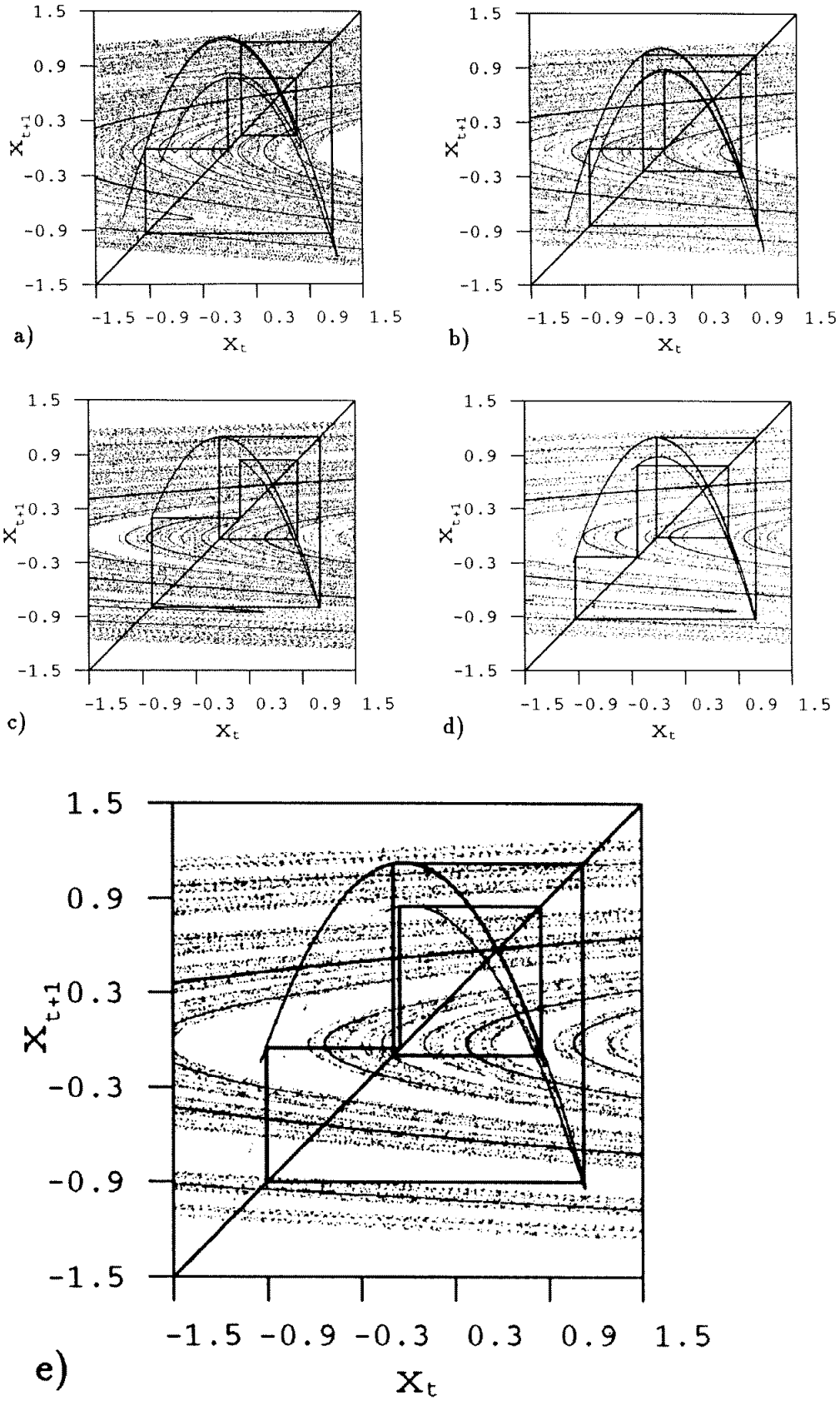

Figure 4.16: The stable period 5 orbit and the stable and unstable manifolds for the Hénon map.
a) $a = 1.465$, $b = 0.25$,

doubled swallow tail crossings of the Lozi map bifurcates at one singular parameter point $a = 1.563\ldots$, $b = 0.380\ldots$, and there is no scaling. Figure 4.15 shows the period 10 orbits from the period doubling of the crossing.

For values of b less than the parameter of the period 5 swallow tail crossing the bifurcation takes place close to the critical point of the fold $f_1(x)$. For larger values of b the critical point on the fold $f_0(x)$ is responsible for the bifurcations. This is the description in the one dimensional bimodal approximation and that the description is valid in the Hénon map is illustrated in the figures 4.16 a), b), c), d) and e). These figures show the stable period 5 orbit, the unstable manifold and parts of the stable manifold at parameter values in the different tails and in the middle of the crossing. The figures 4.16 c) and d) are below the cross and have one point in the stable orbit close to a turning point on the outer fold. In figure a) and b) the orbits have a point close to a turning point on the inner fold of the unstable manifold. When identifying the outer folds with $f_1(x)$ and the inner folds with $f_0(x)$ this is consistent with the one-dimensional approximation. In figure 4.16 e) the orbit is close to both the two turning points.

To further illustrate that the bifurcation is well described by a bimodal one dimensional map, we can plot the unstable manifold in the space (x_t, x_{t+5}). This way to investigate the orbits are discussed in section 4.3.8.

4.3.3 Period 6 orbits

The bifurcation diagram of the period 6 orbits is similar to the period 5 orbit bifurcation diagram but has 3 more orbits. One period 6 orbit is $\overline{100101}$ which is the period doubling of the period 3 orbit. Two orbits; $\overline{101111}$ and $\overline{101110}$ are stable windows in the two chaotic bands. The other 6 orbits have a structure very similar to the period 5 orbits. The two orbits $\overline{100000}$ and $\overline{100001}$ give bifurcations similar to the orbits $\overline{10^k\epsilon}$, $k < 4$. The four orbits $\overline{100\epsilon_1 1\epsilon_2}$ give a swallowtail structure similar to the period 5 swallowtail $\overline{10\epsilon_1 1\epsilon_2}$ and this swallowtail in the symbol plane is drawn in figure 4.17.

4.3.4 Longer periodic orbits

We can also plot the bifurcation plane for longer periodic orbits. To make the pictures readable only the orbits giving swallowtails are drawn. Figure 4.18 give the period 7 swallowtails; $\overline{1000\epsilon_1 1\epsilon_2}$ and $\overline{10\epsilon_1 111\epsilon_2}$. Figure 4.19 shows the period 8 swallowtails; $\overline{10000\epsilon_1 1\epsilon_2}$, $\overline{100\epsilon_1 101\epsilon_2}$, $\overline{100\epsilon_1 111\epsilon_2}$, $\overline{10\epsilon_1 1011\epsilon_2}$ and $\overline{1001\epsilon_1 10\epsilon_2}$, where the last swallowtail is below the diagonal and exists for maps with positive

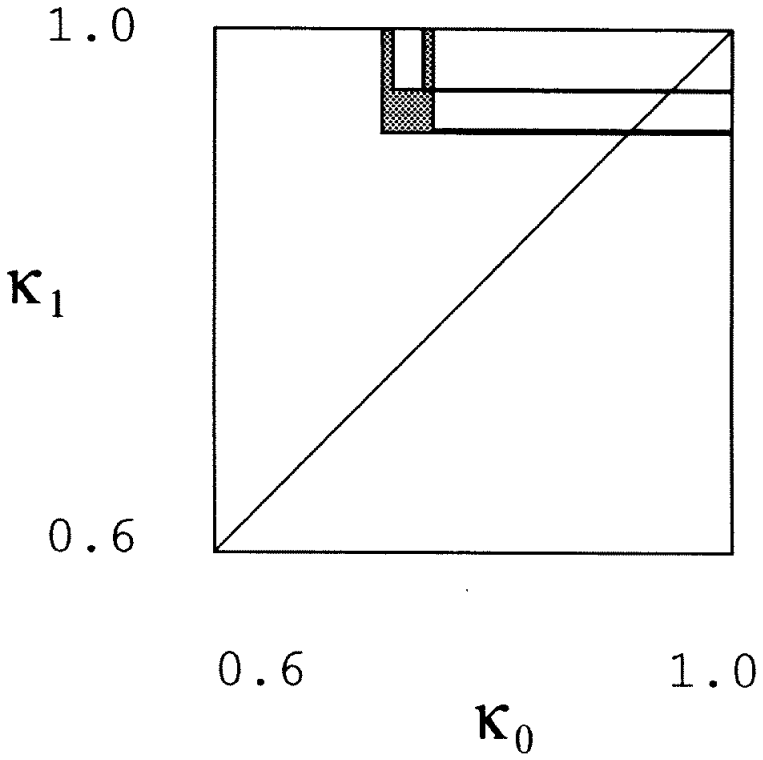

Figure 4.17: The bifurcation lines of the period 6 orbits giving a binary swallow tail in the symbol plane (κ_0, κ_1).

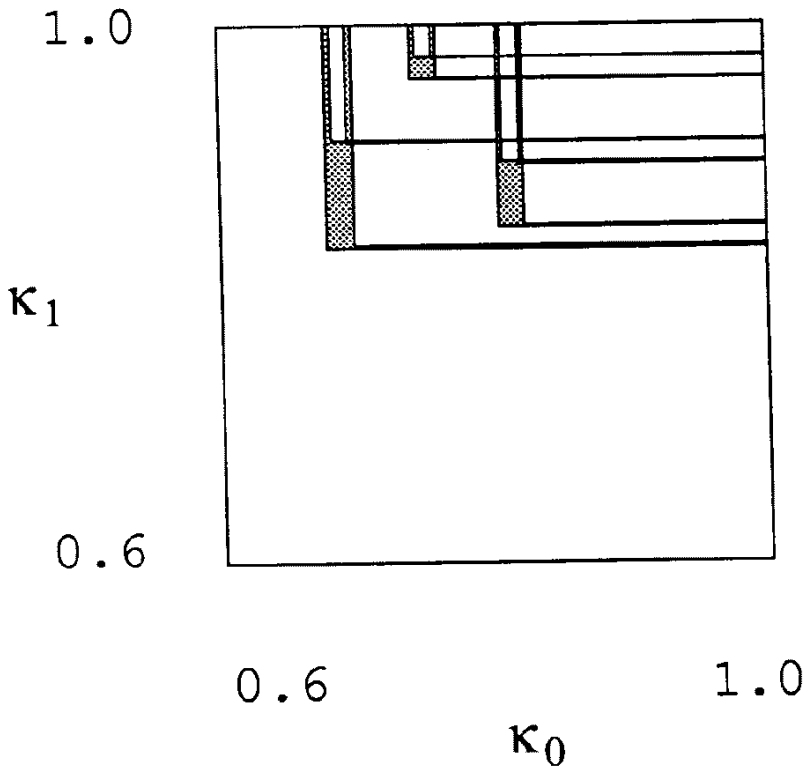

Figure 4.18: The bifurcation lines of the period 7 orbits giving binary swallow tails in the symbol plane (κ_0, κ_1).

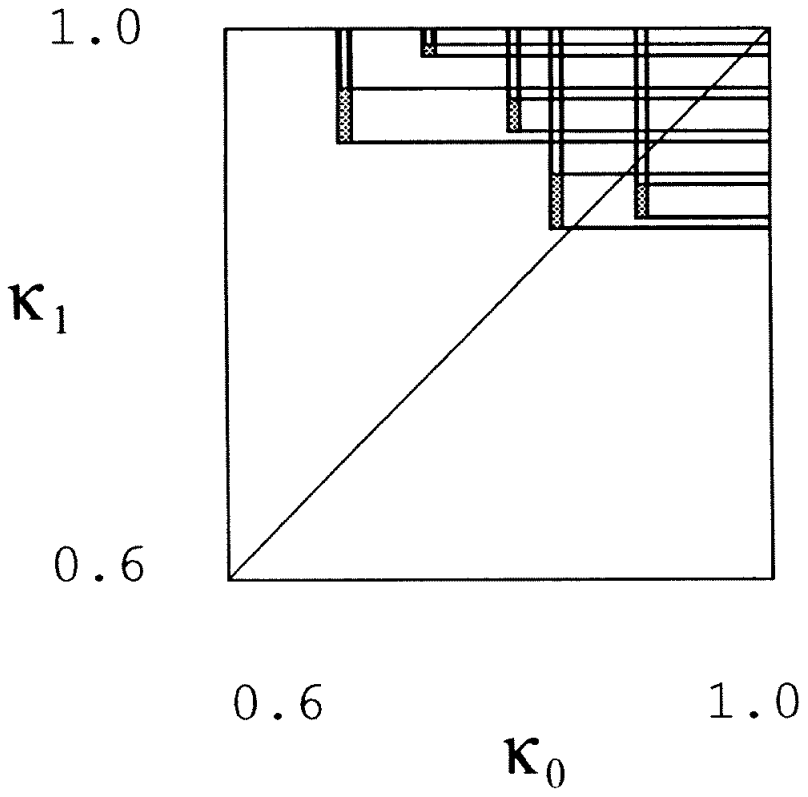

Figure 4.19: The bifurcation lines of the period 8 orbits giving binary swallow tails in the symbol plane (κ_0, κ_1).

$|\mathbb{J}|$ ($b < 0$ for the Hénon and Lozi maps). Figure 4.20 shows the period 9 swallowtails; $\overline{100000\epsilon_1 1\epsilon_2}$, $\overline{1000\epsilon_1 101\epsilon_2}$, $\overline{100\epsilon_1 1001\epsilon_2}$, $\overline{100\epsilon_1 1011\epsilon_2}$, $\overline{10\epsilon_1 11101\epsilon_2}$, $\overline{10\epsilon_1 10111\epsilon_2}$, $\overline{10\epsilon_1 10101\epsilon_2}$, $\overline{10\epsilon_1 11111\epsilon_2}$, $\overline{10011\epsilon_1 10\epsilon_2}$ and $\overline{10001\epsilon_1 10\epsilon_2}$ where the two last exist for positive $|\mathbb{J}|$.

4.3.5 Generic bimodal swallowtails

The most characteristic structure in the bifurcation diagrams in figure 4.9, 4.17, 4.18, 4.19 and 4.20 is the swallowtail crosses. A cross in the bimodal approximation always has two tails crossing the diagonal $\kappa_0 = \kappa_1$ which corresponds to $b = 0$ in the Hénon map. Two windows in the logistic map are then connected at some point for $b \neq 0$ and we can give the generic symbolic description of which two windows in a unimodal map that are connected in the bimodal approximation.

From the one dimensional theory we know that a window in the logistic map has a stable period n orbit with symbolic description $\overline{S} = \overline{s_1 s_2 \cdots s_n}$ where this string is the cyclic permutation giving the largest symbolic value $\tau_i^{\max}(\overline{S}) = \tau(\overline{s_1 s_2 \cdots s_n})$.

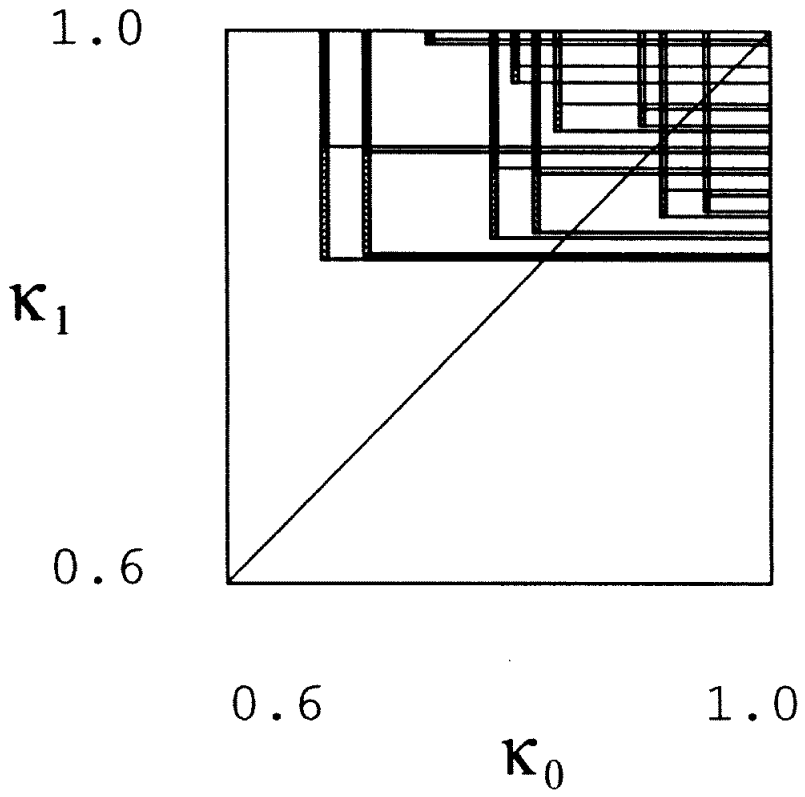

Figure 4.20: The bifurcation lines of the period 9 orbits giving binary swallow tails in the symbol plane (κ_0, κ_1).

The value of s_n changes when the orbit goes through the super-stable point. From the creation of the orbit until the super-stable point, the value of s_n is such that the number of symbol 1's in the string is even. Above the super-stable point s_n changes such that the number of 1's in the string is odd. This because the slope is $+1$ when an orbit is created and -1 when it becomes unstable. At the parameter value where the orbit is created either an orbit of length $n/2$ becomes unstable in a period doubling or an unstable period n orbit is created in a tangent bifurcation. This unstable orbit has the same symbolic description as the stable orbit before the super-stable orbit, that is an even number or 1's. These two orbits can then be described by the string $\overline{s_1 s_2 \cdots s_{n-1}\epsilon_1}$ with $\epsilon_1 \in \{0,1\}$.

The following result states which windows in the unimodal map are connected by a swallowtail cross in the bimodal approximation.

Proposition 1 *Let* $\overline{S} = \overline{s_1 s_2 \cdots s_{n-1}\epsilon}$ *and* $\overline{S'} = \overline{s'_1 s'_2 \cdots s'_{n-1}\epsilon}$, $\epsilon \in \{0,1\}$ *be the symbolic description of the orbits in two windows of the unimodal map. These two windows are the tails from the same bimodal swallowtail cross in a once-folding map if and only if*

$$\begin{aligned}
&s_j = s'_j \quad \textit{for} \quad j \in \{1,2,\ldots,k-1,k+1,\ldots,n-1\} \\
&s_k = 1 - s'_k \\
&s_{k-1} = 1 - s_{n-1} \\
&\tau^{\max}_{s_{n-1}}(\overline{S}) = \tau(\overline{s_1 s_2 \cdots s_{n-1}\epsilon}) \\
&\tau^{\max}_{s_{n-1}}(\overline{S'}) = \tau(\overline{s'_1 s'_2 \cdots s'_{n-1}\epsilon}) \\
&\tau^{\max}_{1-s_{n-1}}(\overline{S}) = \tau(\overline{s_{k+1} s_{k+2} \ldots s_{n-1}\epsilon s_1 s_2 \cdots s_k}) \\
&\tau^{\max}_{1-s_{n-1}}(\overline{S'}) = \tau(\overline{s'_{k+1} s'_{k+2} \ldots s'_{n-1}\epsilon s'_1 s'_2 \cdots s'_k})
\end{aligned} \tag{4.33}$$

A slightly different way to state this is

Proposition 2 *A bimodal swallowtail of the once-folding map has the symbolic description*

$$\overline{S} = \overline{s_1 s_2 \cdots s_m 0 \epsilon_1 s_{m+3} s_{m+4} \ldots s_{n-2} 1 \epsilon_2} \tag{4.34}$$

with

$$\begin{aligned}
\tau^{\max}_1(\overline{S}) &= \tau(\overline{s_1 s_2 \cdots s_m 0 \epsilon_1 s_{m+3} s_{m+4} \ldots s_{n-2} 1 \epsilon_2}) \\
\tau^{\max}_0(\overline{S}) &= \tau(\overline{s_{m+3} s_{m+4} \ldots s_{n-2} 1 \epsilon_2 s_1 s_2 \cdots s_m 0 \epsilon_1})
\end{aligned} \tag{4.35}$$

The crossing is in the map with reflection ($b > 0$ for Hénon) if $\tau^{\max}(\overline{S}) = \tau^{\max}_1(\overline{S})$ *and the crossing is in the map without reflection ($b < 0$ for Hénon) if* $\tau^{\max}(\overline{S}) = \tau^{\max}_0(\overline{S})$

As a short notation we write $\overline{A 0 \epsilon_1 B 1 \epsilon_2} = \overline{s_1 s_2 \cdots s_m 0 \epsilon_1 s_{m+3} s_{m+4} \ldots s_{n-2} 1 \epsilon_2}$

4.3.6 Symbols of period doublings of swallowtails

Each period n swallowtail crossing $\overline{A0\epsilon_0 B1\epsilon_1}$ has a period doubling structure. The two stable orbits have a period doubling and become the outer bounds of two new swallowtail crossings with period $2n$ orbits. In figure 4.13 the two period 10 swallowtail crossings and the stable period 5 orbits bifurcation lines are drawn in the symbol plane. The period n swallowtail bifurcates into 2^k swallowtails of length $2^k n$ giving a family of swallowtails.

The symbolic description of an orbit in the unimodal period doubling bifurcation is obtained by repeating the shorter symbol sequence twice and change the last symbol (a harmonics). This symbol corresponds to the point close to the critical point.

For the swallowtail crossings we take the symbolic string of the stable orbit and write this string twice

$$\overline{A0\epsilon_0 B1\epsilon_1 A0\epsilon_0' B1\epsilon_1'} \tag{4.36}$$

with $\epsilon_0' = \epsilon_0$ and $\epsilon_1' = \epsilon_1$. We now have two points close to critical points. By changing ϵ_1' from ϵ_1 to $(1-\epsilon_1)$ we make a point in an orbit crossing the critical point on map 1; x_c^1. This gives the symbolic description of one new stable orbit. When we change ϵ_0' from ϵ_0 to $(1-\epsilon_0)$ this corresponds to moving a point in an orbit across the point x_c^0 and we get the symbolic description of the other stable orbit. Changing both ϵ_1' and ϵ_0' gives the unstable orbit in the middle of the swallow tail.

With the two choices of ϵ_1 and ϵ_0 that give the two stable period n orbits, this is the symbolic description of the 6 new orbits in the two period $2n$ swallowtail crosses.

4.3.7 Bimodal MSS ordering

The ordering of orbits along the parameter of the unimodal map follows the Metropolis-Stein-Stein (MSS) ordering. In ref. [147] MSS gave a table (table I) with the ordering of the periodic orbits of length 7 and shorter. We can now rewrite this table and include the ordering of both folds in our bimodal approximation of the once-folding map. In table 4.1 we give this table and we use here both the MSS notation and the notation we use.

MSS uses the symbols R and L for a point to the right or left of the critical point. This is identical to 1 and 0 in our notation, but they only write the first $n-1$ symbols for a period n orbit given in the column P_i in table 4.1. They discuss unimodal maps and the last symbol only distinguishes between the stable and the unstable

i	k_i	P_i	S_i	$\tau_{1,i}^{\max}$	S_i	$\tau_{0,i}^{\max}$
$21'$			$\overline{0000010}$	$.\overline{00000111111100}$		
$20'$			$\overline{000010}$	$.\overline{000011111100}$		
$18'$			$\overline{00010}$	$.\overline{0001111100}$		
$14'$			$\overline{0010}$	$.\overline{00111100}$		
$1'$					$\overline{01}$	$.\overline{0110}$
$7'$			$\overline{010}$	$.\overline{011100}$		
$13'$			$\overline{0100110}$	$.\overline{01110111000100}$		
$15'$			$\overline{1100010}$	$.\overline{10000110111100}$		
$8'$			$\overline{110010}$	$.\overline{100011011100}$		
$2'$					$\overline{1101}$	$.\overline{10010110}$
$12'$					$\overline{110100}$	$.\overline{100111011000}$
$3'$					$\overline{111101}$	$.\overline{101001010110}$
$11'$					$\overline{1111100}$	$.\overline{10101110101000}$
$4'$					$\overline{1110101}$	$.\overline{10110010100110}$
$10'$					$\overline{11100}$	$.\overline{1011101000}$
$16'$					$\overline{111000}$	$.\overline{101111010000}$
$19'$					$\overline{1110000}$	$.\overline{10111110100000}$
$17'$					$\overline{1010001}$	$.\overline{11000010011110}$
$5'$					$\overline{10101}$	$.\overline{1100100110}$
1	2	R	$\overline{10}$	$.\overline{1100}$		
$9'$					$\overline{1010100}$	$.\overline{11001110011000}$
$6'$					$\overline{1011101}$	$.\overline{11010010010110}$
2	4	RLR	$\overline{1011}$	$.\overline{11010010}$		
3	6	RLR^3	$\overline{101111}$	$.\overline{110101001010}$		
4	7	RLR^4	$\overline{1011110}$	$.\overline{11010110010100}$		
5	5	RLR^2	$\overline{10110}$	$.\overline{1101100100}$		
6	7	RLR^2LR	$\overline{1011011}$	$.\overline{11011010010010}$		
7	3	RL			$\overline{100}$	$.\overline{111000}$
8	6	RL^2RL			$\overline{100101}$	$.\overline{111001000110}$
9	7	RL^2RLR	$\overline{1001010}$	$.\overline{11100110001100}$		
10	5	RL^2R	$\overline{10011}$	$.\overline{1110100010}$		
11	7	RL^2R^3	$\overline{1001111}$	$.\overline{11101010001010}$		
12	6	RL^2R^2	$\overline{100110}$	$.\overline{111011000100}$		
13	7	RL^2R^2L			$\overline{1001100}$	$.\overline{11101110001000}$
14	4	RL^2			$\overline{1000}$	$.\overline{11110000}$
15	7	RL^3RL			$\overline{1000101}$	$.\overline{11110010000110}$
16	6	RL^3R	$\overline{100011}$	$.\overline{111101000010}$		
17	7	RL^3R^2	$\overline{1000110}$	$.\overline{11110110000100}$		
18	5	RL^3			$\overline{10000}$	$.\overline{1111100000}$
19	7	RL^4R	$\overline{1000011}$	$.\overline{11111010000010}$		
20	6	RL^4			$\overline{100000}$	$.\overline{111111000000}$
21	7	RL^5			$\overline{1000000}$	$.\overline{11111110000000}$

Table 4.1: The Metropolis-Stein-Stein ordering extended to a two fold description of the once-folding map.

orbit born at the same parameter value. As we also discuss bifurcations where orbits bifurcates together with other partners we have to include all n symbols. In table 4.1 we have chosen to let the last symbol be the symbol 0 or 1 such that the symbol string has an odd number of 1's and this is the description of the orbit that is stable for some parameter values in a smooth map.

A number i is used by MSS to identify the different orbits and we have in table 4.1 introduced a notation i' which is the same orbit as i but with the cyclic rotation giving the bifurcation on the other fold. The length of the orbit is denoted k_i by MSS.

The way the MSS table for the unimodal map is used is that the ordering in the table is the same as the ordering at the parameter axis in a unimodal map. The extended MSS table has two columns with respectivally $\tau_{1,i}^{\max}$ and $\tau_{0,i}^{\max}$ and this give two different orderings. The ordering in column $\tau_{1,i}^{\max}$ gives the ordering of the orbits bifurcating at map 1 when map 0 has $\kappa_0 = 1$. The other column $\tau_{0,i}^{\max}$ gives the ordering of the orbits bifurcating at map 0 when map 1 has $\kappa_1 = 1$. This is a table description of the bifurcations along the two lines $\kappa_0 = 1$ and $\kappa_1 = 1$ in the symbolic parameter plane. A swallowtail bifurcation in the symbolic parameter plane imply that the ordering is different in the two columns in table 4.1. We find that the two orbits in the period 5 swallowtail crossing is $i = 5$ and $i = 10$ which according to $\tau_{1,i}^{\max}$ is ordered with $i = 5$ before $i = 10$ but according to the $\tau_{0,i}^{\max}$ value $i = 10'$ comes before $i = 5'$ and the orbits has to cross each other at some point in the parameter space.

This table may be helpfull for people aquanted with the MSS theory, but the drawings of bifurcation lines in the symbolic parameter space gives more information and we prefer to use this.

4.3.8 The n-th return plot

To study the bifurcation of a period n orbit in a one dimensional map we often plot the n-th iterate of the map f. In the space $(x, f^{(n)})$ the period n orbit is a fixed point and by finding when $f^{(n)}$ crosses the diagonal we find the bifurcations of the map. In a once-folding two dimensional map we can try to apply the same technique, but in this case we do not have one function $f(x_t)$ but a fractal manifold which gives x_{t+1} as a function $f(x_t)$ that also depends on x_{t-1}.

The chaotic attractor for $a = 1.6$, $b = 0.14$ is drawn in the two planes (x_t, x_{t+1}) and (x_t, x_{t+5}) in figure 4.21 a) and b). These parameter values are between the tails of the period 5 swallowtail in figure 4.11 where all the four orbits in the family $\overline{10\epsilon_1 1\epsilon_2}$ exist. We then know that 20 of the points where one of the lines in the

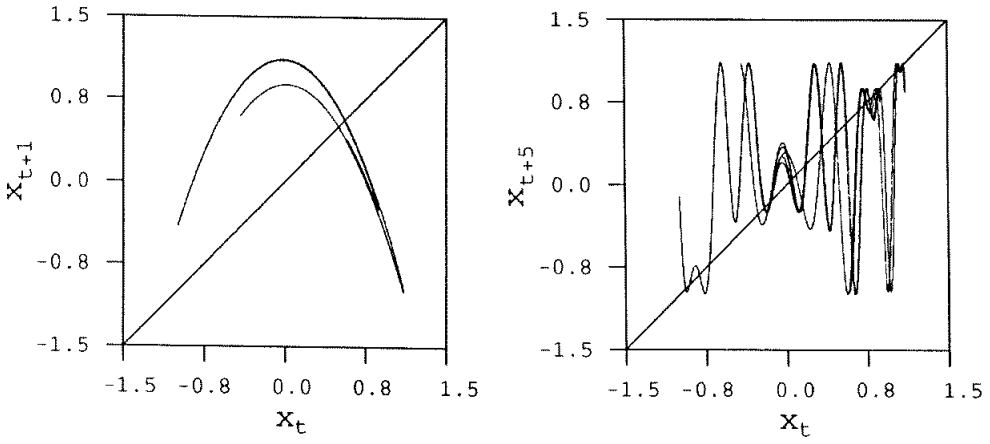

Figure 4.21: The chaotic attractor plotted in (x_t, x_{t+1}) and (x_t, x_{t+5}) with parameters $a = 1.6$ $b = 0.14$.

fractal in figure 4.21 a) crosses the diagonal, are points in period 5 orbits. A period 5 orbit is 5 fixed points in this plot. The 20 fixed points are on different folds and most of the crossings do not correspond to real fixed point. The fixed point are the points where the lines of the fractal crosses the diagonal $x = y = z$ in a three dimensional plot (x_t, x_{t+5}, x_{t+10}) and the picture in (x_t, x_{t+5}) is only a projection of this space. We can not show the exact bifurcations in this two dimensional plot but the picture is useful as a qualitative description of the bifurcation.

Instead of trying to find the exact curves of the chaotic attractor, we draw a small segment of the unstable manifold of the fixed point $\overline{1}$ which gives one single curve in the (x_t, x_{t+5}) plot. This gives an acceptable *qualitative* description of the bifurcation. In figures 4.22 a), b) and c) this curve is drawn together with the fixed points corresponding to period 5 orbits in the Hénon map. We have drawn one of the five points for each orbit with markers of different shapes. The markers for the different orbits are $\circ$ for $\overline{10111}$, $+$ for $\overline{10110}$, $\times$ for $\overline{10010}$ and $\triangle$ for $\overline{10011}$. Figure 4.22 b) has parameter values $a = 1.6$ $b = .14$ which are between the inner tails of the swallowtail crossing in figure 4.11 and all four period 5 orbits exist. Letting b increase or decrease one crosses tails from the swallowtail crossing and two orbits get pruned. Figures 4.22 a) and c) show that the pruning of the two orbits follows from the different possible changes of the $f^{(n)}$ curve. The two minimum points in figure 4.22 have the same height and are controlled by one parameter while the second parameter controls the height of the maximum point.

These figures shows how we can obtain qualitative information of bifurcations by a simple return map and for the Hénon map we find that this information is

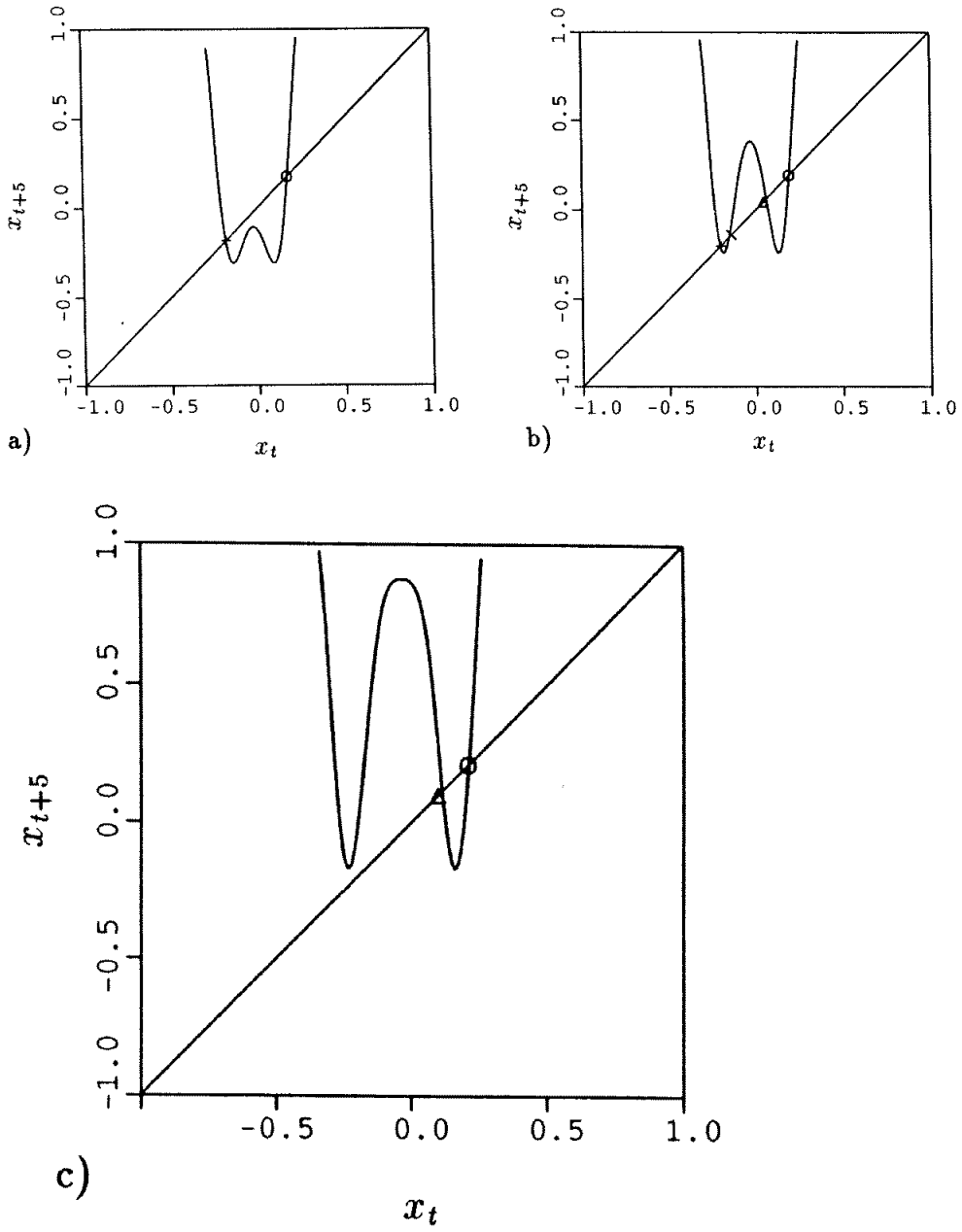

Figure 4.22: The fifth return map of a segment of the unstable manifold and points in the period 5 orbit; $a = 1.6$, a) $b = 0.115$; b) $b = 0.14$ and c) $b = 0.17$.

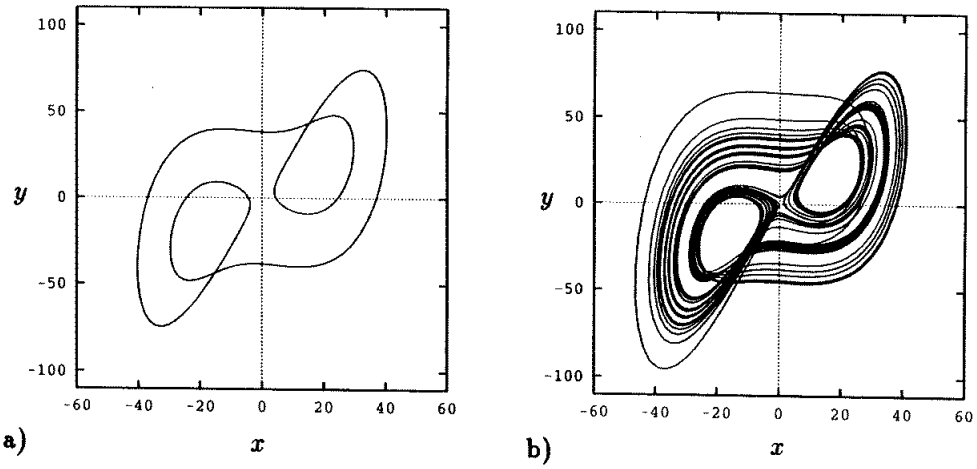

Figure 4.23: The attractor of the Lorenz model projected at the (x, y) plane, $\sigma = 10$, $b = 8/3$, a) $r = 163.5$; b) $r = 135.0$.

consistent with the detailed analysis based on the symbolic dynamics.

4.3.9 The n-th map of the Lorenz model

To illustrate the n-th iterated map on a more complicated system, we have calculated return maps also for the Lorenz system [65, 136, 186]. The Lorenz system is given by the first-order differential equations

$$\begin{aligned} \dot{x} &= -\sigma x + \sigma y \\ \dot{y} &= -xz + rx - y \\ \dot{z} &= xy - bz \end{aligned} \tag{4.37}$$

The bifurcations of this map have often been studied keeping the parameters σ and b fixed to the values $\sigma = 10$ and $b = 8/3$, and changing the parameter r [81, 186]. This gives parameter windows with a stable periodic orbit, and a simple return plot yields qualitative information on what kind of bifurcation structure these windows belongs to in a higher dimensional parameter space.

In the largest window on the r axis is the orbit drawn in figure 4.23 a) stable. The figure is the projection of the orbit to the (x, y) space. When the parameter r increases from this value, $r = 163.5$, the orbit will disappear, while for smaller values of r the orbit becomes unstable. Figure 4.23 b) shows a segment of the chaotic attractor for $r = 135.0$. These plots of the orbit in the (x, y) plane do not give much information of which kind of approximate one dimensional map the orbit locally experiences. To find this we take as a Poincaré map the x_t values where the orbit crosses the x-axis from a positive to a negative value of y. In this Poincaré

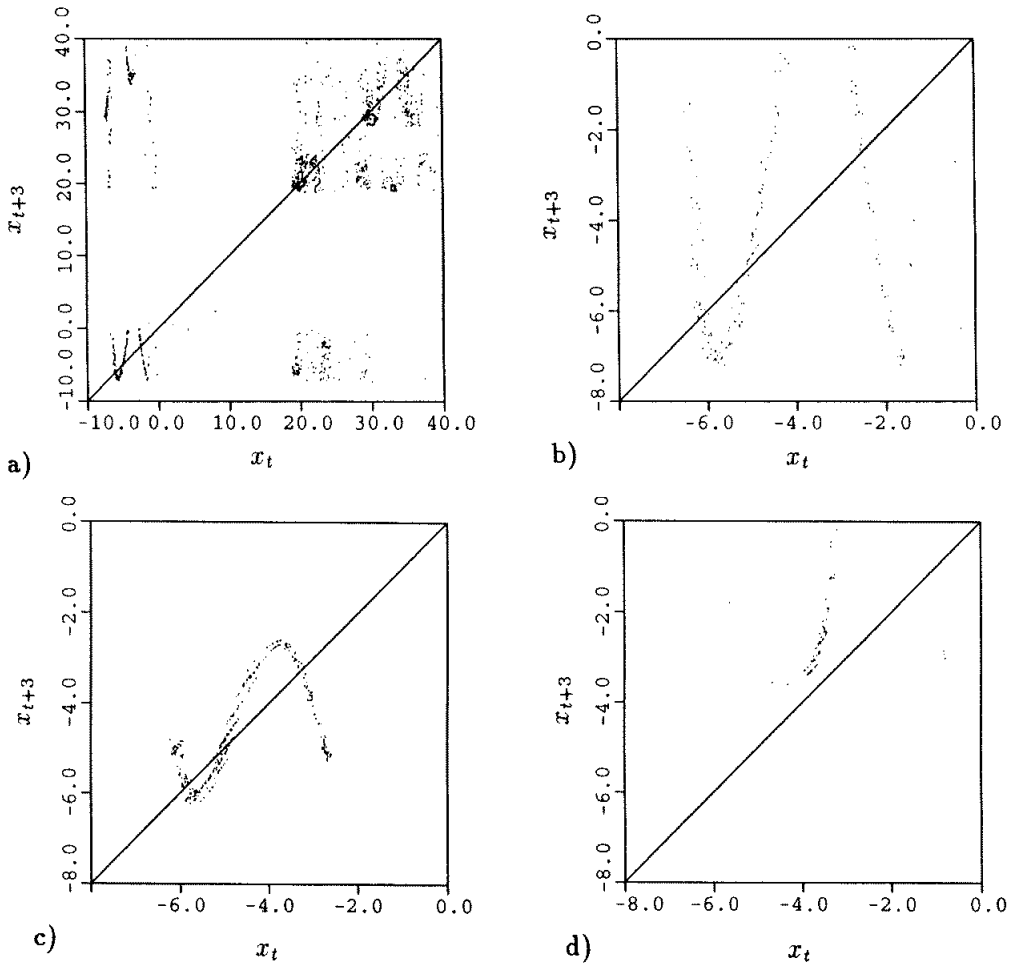

Figure 4.24: The third return map (x_t, x_{t+3}) of the Lorenz model, $\sigma = 10$, $b = 10/3$, a) $r = 135.0$ and the whole Poincaré plane; b) a magnification of a) with the same parameter values; c) $r = 145.0$; d) $r = 163.5$.

map the orbit in figure 4.23 a) is a period 3 orbit and we choose to plot the orbits in the plane (x_t, x_{t+3}) where the period 3 orbit is a fixed point. The time index t is here the integer counting intersections with the Poincaré plane and not the time in the differential equations (4.37).

Points of a chaotic orbit in the Lorenz system are plotted in (x_t, x_{t+3}) in figure 4.24. In figure 4.24 a) all points are plotted for parameter $r = 135.0$, and the structure down and left in this plot is magnified in figure 4.24 b). We find here pictures which are similar to the bimodal bifurcation pictures for the period 5 orbit in the Hénon map, figure 4.21. The points in figure 4.24 b) strongly suggest a bimodal map were there is two independent critical points. The two minimum points seems to be of the same height which excludes a three modal map bifurcation from being

important. By increasing r to 145.0, figure 4.24 c), we find a typical bimodal map which here is restricted to a band (analog to the chaotic band before the period 3 crisis bifurcation in the logistic map). Increasing the parameter further, we obtain figure 4.24 d) for $r = 168.0$, where the orbit does not exist and the structure is very similar a tangent bifurcation in a one dimensional map. There seems to have been a transition to a locally unimodal map here.

From these figures it is not difficult to predict that any two dimensional scan of the parameter space has to give a bimodal swallowtail as the bifurcation of this orbit, and that the line with $\sigma = 10$ and $b = 8/3$ is close to but not exactly in the middle of the swallow tail crossing since the "function" figure 4.24 c) is slightly asymmetric around the fixed point. We expect that with further investigations of this kind and better understanding of the symbols of the system one can construct the bifurcations in a topological parameter space also for the Lorenz system. A simple comparison of the symbolic description of stable windows in the Lorenz map and a cubic map has been done by Hao Bai-lin [106].

We belive that such a numerical procedure can be useful for understanding the bifurcation structure for many low dimensional chaotic systems and may be useful in finding a symbolic description. Further investigations is necessary to test how useful this method is in describing bifurcations and for the understanding of the structure of the non-wandering set of the systems.

4.4 Four unimodal maps approximation

The two-fold description cannot explain all swallowtails observed in the Hénon map [153]. To explain other structures we have to approximate the Hénon map with 4 unimodal maps which we refer to as a second order approximation. The four maps approximation reproduces all the swallowtails we found by the bimodal map approximation as a special case, but it also yields more complicated structures. We know from section 2.2 that a general trimodal one dimensional map already yields rather complicated diagrams like figure 2.20, and we can hardly expect to be able to draw the complete bifurcation diagram for this special four-modal map. We can however trace out some subspaces of the 4 dimensional topological parameter space and use these to explain the bifurcations found in numerical experiments. The four-modal map has co-dimension 4 and all the possible bifurcation structures in the four dimensional parameter space cannot be realized in the Hénon map that has only 2 parameters. It should in principle be possible to construct a Hénon like map with 4 parameters that realized all possible bifurcations. We show below that when we add one new parameter c with a x^4 term to the Hénon function, we obtain bifurcations not existing in the Hénon. These are other possible realizations of the bifurcations in the four-dimensional symbolic parameter space.

This variant of the Hénon map is the map

$$x_{t+1} = 1 - ax_t^2 - cx_t^4 - bx_{t-1} \tag{4.38}$$

For $c > 0$ this is a once-folding map. If $c < 0$ the map is three-folding but for $-1 << c < 0$ most of the bifurcations are described by the bifurcation diagrams of the once-folding map.

An additional term with a fourth parameter yields further bifurcation structure (not investigated here). A good choice of four parameters should reproduce all bifurcations predicted by the four-dimensional topological parameter space and also other smaller bifurcation structures in addition to this. A fifth independent parameter in the map cannot yield further bifurcations described by the four dimensional symbolic parameter space, but any new bifurcations obtained here belongs to a higher order in the one dimensional map approximations. The bifurcations we find in the Hénon map parameter plane should be topological equivalent to a 2 dimensional cut through the 4 dimensional symbolic parameter space.

Let us denote the four unimodal maps by 10, 00, 01 and 11. Point x_t in the non-wandering set with symbolic description $\ldots s_{t-3}s_{t-2}s_{t-1}s_ts_{t+1}s_{t+2}s_{t+3}\ldots$ lies on the map $s_{t-2}s_{t-1}$ and the ordering of the 4 maps in the phase space follows from the folding of the horseshoe. Each map has a critical point with an associated

topological parameter $\kappa_{s's}$ obtained by the kneading sequence of the critical point. The ordering of the maps and the values $\kappa_{s's}$ is found by applying the horseshoe map three times on a rectangle in the (x_t, x_{t+1}) space, as shown in figures 3.4 and 3.9 and we find that the ordering for $b > 0$ is

$$\kappa_{10} < \kappa_{00} < \kappa_{01} < \kappa_{11} \tag{4.39}$$

and for $b < 0$

$$\kappa_{01} < \kappa_{11} < \kappa_{10} < \kappa_{00} \tag{4.40}$$

From our experience with the trimodal maps we expect to find many swallowtail crossings that sometimes combine together into a large complicated crossing, and cusp bifurcations with two tails such that an orbit can change symbolic dynamics without becoming stable.

4.4.1 Period 6 swallowtails

An example of a cusp bifurcation where the modality of the approximation changes from 4 to 2 is given in figure 4.25 (cf. figure 6.32 in Mira [153]). The ordinary swallowtail cross in figure 4.25 a) is the bimodal cross from the symbolic parameter plane in figure 4.17. The tail $\overline{11100\epsilon}$ from this cross bifurcates into a cusp similar to one of the cusp in figure 2.14. In the isolated window to the left in figure 4.25 a) the symbolic dynamics of the stable orbit changes without any visible trace in the (a, b) plane. This implies, as pointed out in ref. [107] that an unstable orbit can change symbolic dynamics moving adiabatically along a loop in the parameter plane.

The bimodal swallowtail is described by figure 4.17, and we can also describe other structures in the symbolic space $(\kappa_{00}, \kappa_{01}, \kappa_{10}, \kappa_{11})$. From figure 4.25 a) we find that the two tails from the bimodal swallowtail that do not cross the $b = 0$ axis, $\overline{11100\epsilon}$ and $\overline{10100\epsilon}$, bifurcate along the κ_{00} axis since $s_{-2}s_{-1} = s_4 s_5 = 00$. The second tail from the simple swallow and the uppermost part of the isolated window bifurcate along the κ_{10} axis. In figure 4.27 the bifurcation lines of these orbits are drawn. The unstable orbit $\overline{111001}$ is common for two tails, with the usual associated cusp structure. At this cusp point we have drawn a dashed line to indicate that this cusp is at a point where the four modal map changes into a two modal map. To understand that this is a topological feature we have to consider in detail the maximum and minimum points in the four modal map.

The Biham-Wenzel method gives the bifurcation lines for the different symbol strings drawn in figure 4.26. We find by comparing the figures that the symbolic description of the two tails from the simple cusp in figure 4.25 b) has symbolic

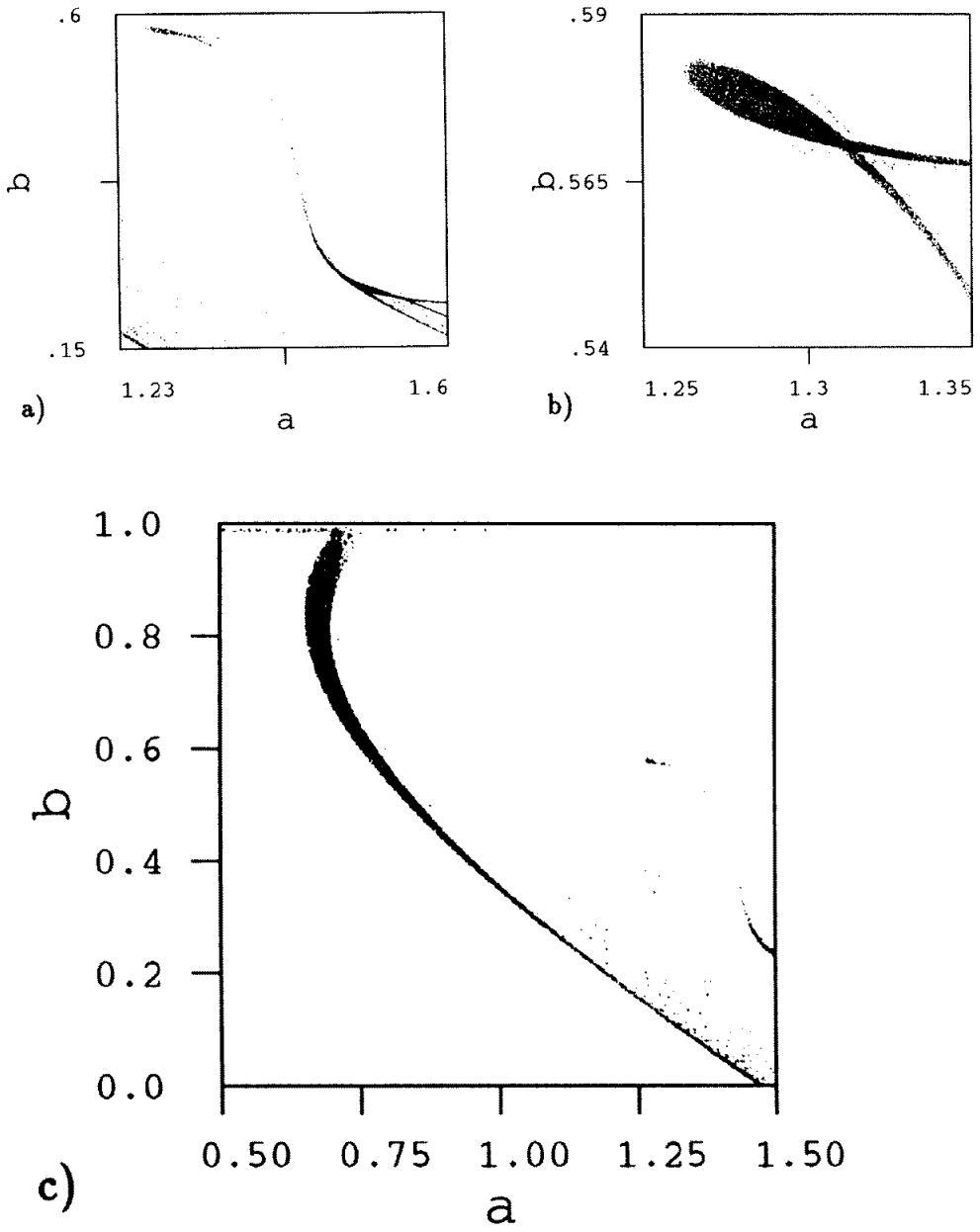

Figure 4.25: The bifurcation of the period 6 orbits in the Hénon map in the parameter space (a, b). a) The stable windows. b) The simple cusp magnified. c) The simple stable window starting as $\overline{10111\epsilon}$ when $b = 0$.

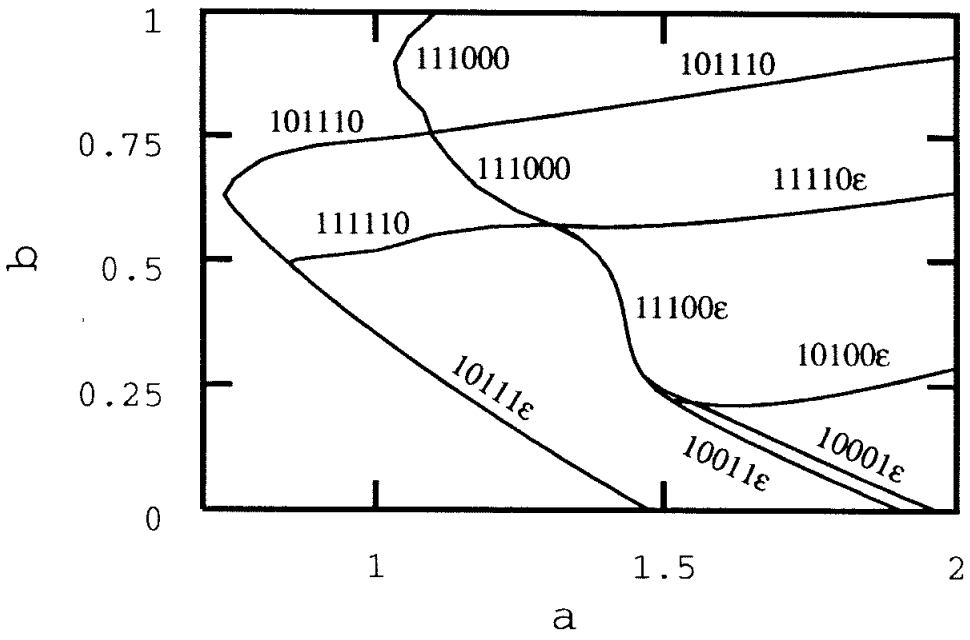

Figure 4.26: The bifurcation of the period 6 orbits in the Hénon map calculated with the complex Biham-Wenzel method.

description $\overline{11100\epsilon}$ and $\overline{11110\epsilon}$. Along the $\overline{11110\epsilon}$ tail the two orbits are close to the maximum point of the map 10, the lowest map in the 4 modal approximation (4.39). The iterate of this maximum point is the minimum point connecting the maps 00 and 01. The symbolic description of this minimum point is the shifted symbol string of the symbolic description of the maximum point on map 10:

$$\sigma(\overline{11110\epsilon}) = \overline{1110\epsilon 1} \tag{4.41}$$

The tail $\overline{11100\epsilon}$ has the two orbits close to the maximum point of the map 00. At the point where the two tails meet we find that the unstable orbit $\sigma(\overline{111100}) = \overline{111001}$ is common for the two tails and we have a cusp bifurcation. Note that the symbolic description of the point on this unstable orbit close to the minimum point is $\overline{111001}$, and at the same time the symbolic description of the maximum point is also $\overline{111001}$. This means that this cusp point is a bifurcation point where the maximum point of the map 00 merges with the minimum point on the same map and the critical point of map 00 disappears. Also the minimum point disappear and since this is an image of the maximum point on map 10 then also the independent critical point on map 10 disappears.

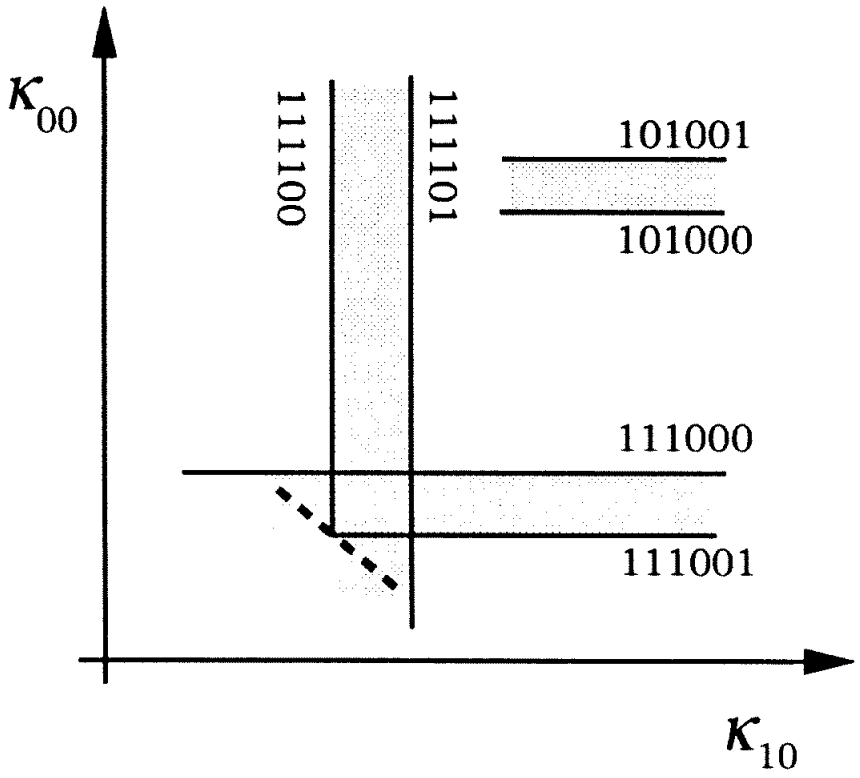

Figure 4.27: The bifurcation lines of some period 6 orbits in the sub-plane $(\kappa_{10}, \kappa_{00})$ of the topological parameter plane.

Proposition 3 *At the parameter values ($b > 0$) where the kneading sequences from the two maps 00 and 10 satisfy*

$$K_{00} = \sigma(K_{10}) \tag{4.42}$$

there is a bifurcation from a four-modal to a two-modal map.

We divide the isolated cusp bifurcations into two types; type 1 where the stable orbit exists around the singular point and type 2 where the parameter values with a stable orbit is a cusp ending in the singular point. With this definition we have the following proposition:

Proposition 4 *If K_{10} is a periodic string, and $K_{00} = \sigma(K_{10})$ then there is a cusp bifurcation of an periodic orbit in the parameter space. If the number of symbols 1 in the repeating string is even then it is a cusp of type 1, and if the number of symbol 1 in the repeating string is odd then it is a cusp of type 2.*

For the period 6 example considered here we have

$$K_{10} = 111100111100111100\ldots \tag{4.43}$$
$$K_{00} = 111001111001111001\ldots = \sigma(K_{10}) \tag{4.44}$$

when we have the topological parameter values

$$\kappa_{10} = 0.\overline{101000} \tag{4.45}$$
$$\kappa_{00} = 0.\overline{101110} \tag{4.46}$$

The number of 1's in this periodic orbit is even and we have a cusp of type 1, with a stable orbit surrounding the cusp point in the parameter space (a, b). The two types are illustrated by the fixed point bifurcation in the trimodal map in section 2.2.

The bifurcation of the period 6 orbits in the Lozi map is drawn in figure 4.28. In this map there are no cusp bifurcation and one crossing is on the $b = 1$ line.

For $b < 0$ ($\det \mathbb{J} > 0$) we have the same propositions with the strings $K_{11} = \sigma(K_{01})$.

The bifurcation lines for the Lozi map is drawn in figure 4.28. Because the manifolds are piecewise linear this map has not any cusp bifurcations. We find in this figure that the Lozi map does not have the bimodal swallowtail but a four-modal swallowtail crossing $\overline{10\epsilon_1 11\epsilon_2}$ in the $(\kappa_{10}, \kappa_{11})$ plane.

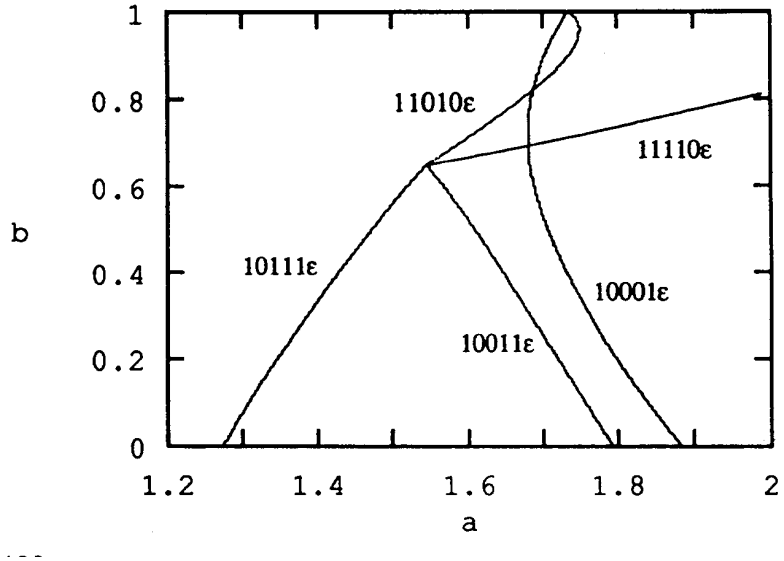

Figure 4.28: The bifurcation lines for period 6 orbits in the Lozi map.

4.4.2 Period 4 orbit cusp bifurcation

The period 4 orbits $\overline{1000}$, $\overline{1001}$ and $\overline{1011}$ have a type 1 cusp bifurcation in the symbolic parameter space $(\kappa_{10}, \kappa_{00})$ in figure 4.29. The unstable orbit $\overline{1001}$ is the common orbit in the two tails. This cusp is exactly on the line $b = 1$. It was showed by Mira [153] that this is because there is a symmetry in the symbol string $\overline{1001}$ ("self-adjoint cycle"). In the n-modal map approximation is it not obvious why this cusp is on the area preserving line, but this symmetry is visible in the symbol plane (γ, δ) and we return to this question in section 5.4. The bifurcation lines for the Lozi map is given in figure 4.30 and figure 4.31 shows the bifurcation lines in the Hénon map. The Biham-Wenzel method in figure 4.31 b) converges the same way for this cusp as for the cusps in the dissipative region. For $b > 1$ the tail consists of an orbit unstable in two directions and by iterating backward the orbit is an attractor. The bifurcation diagram is sketched in figure 4.31 a). There is also additional structures close to this cusp, cf. Mira [153].

4.4.3 Bifurcation of period 8 orbits

Another example of bifurcations in the Hénon map that is explained by the four-modal approximation is the bifurcation structure in figure 4.32. This structure has a complexity comparable to the period 3 orbits in the trimodal map in figure 2.22. Instead of trying to draw a complete four dimensional topological parameter space, we find the symbolic description of the structures and show that this is possible

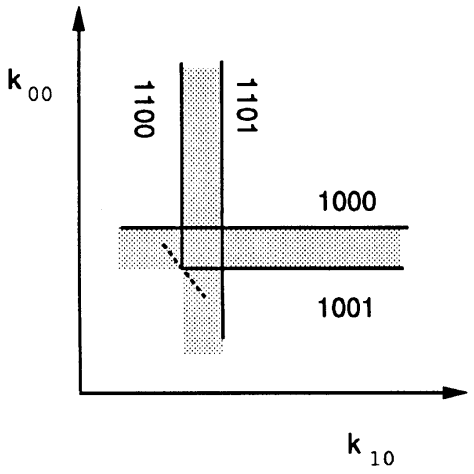

Figure 4.29: The bifurcation of the orbits $\overline{1000}$, $\overline{1001}$ and $\overline{1011}$ in the symbolic parameter plane $(\kappa_{10}, \kappa_{11})$.

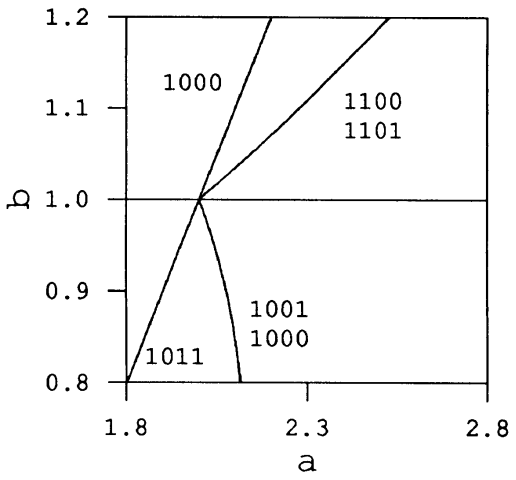

Figure 4.30: The bifurcation curves of period 4 orbits in the Lozi map.

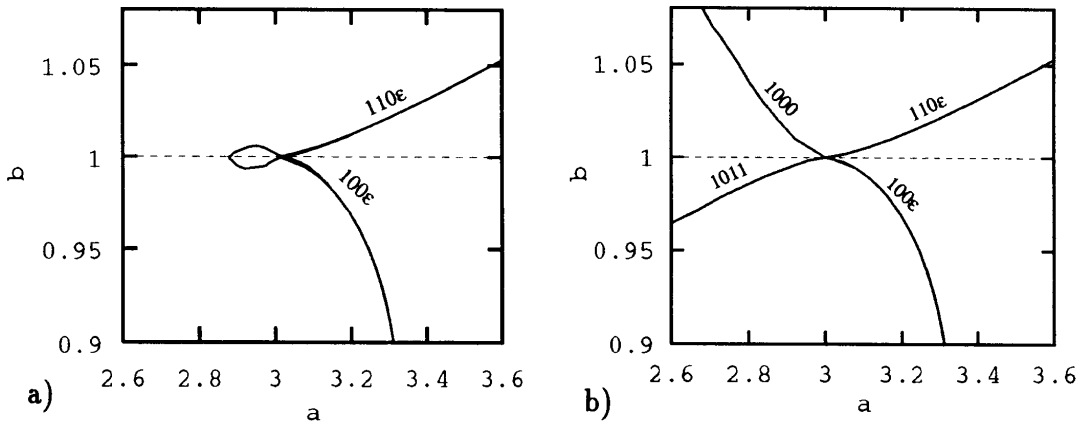

Figure 4.31: The bifurcation curves of the period 4 orbits in the Hénon map. b) Bifurcation curves from the BW-method.

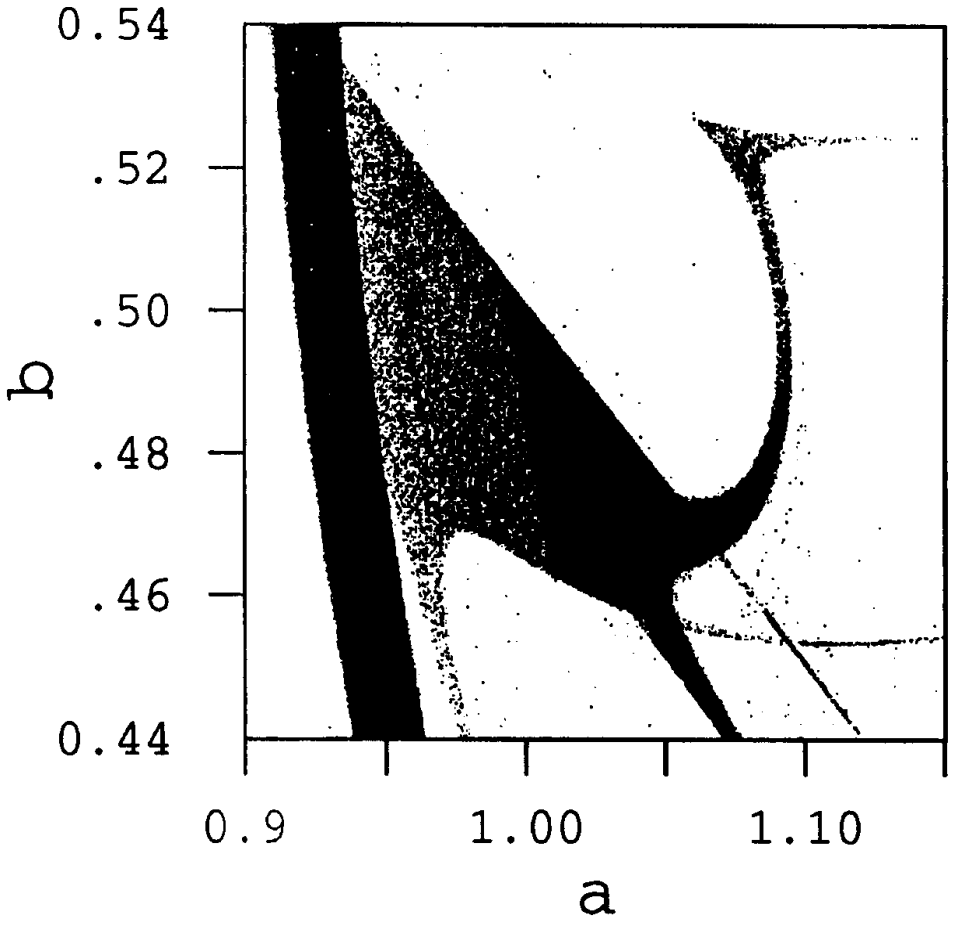

Figure 4.32: The parameter values with stable period 8 orbits in the Hénon map in the parameter space (a, b).

bifurcations in a two dimensional subspaces of the symbolic symbol space. We then perturb the Hénon map with a cx^4 term, and show the transitions to other possible bifurcations in the parameter plane as c varies.

In figure 4.32 there is one window which is a simple almost vertical strip in the left side of the plot. This is the period 8 orbit $\overline{10111010}$ originating from the period doubling family of the fixed point. This orbit is bifurcating along the κ_{01} axis in the symbolic parameter space and is not connected with the other structure in the figure and we will not discuss this any more.

In figure 4.33 the bifurcation lines found by the complex Biham-Wenzel method is drawn in the (a, b) parameter plane. We assume that when these bifurcation lines coincide with the tails of stable orbits in figure 4.32 this is the correct symbolic

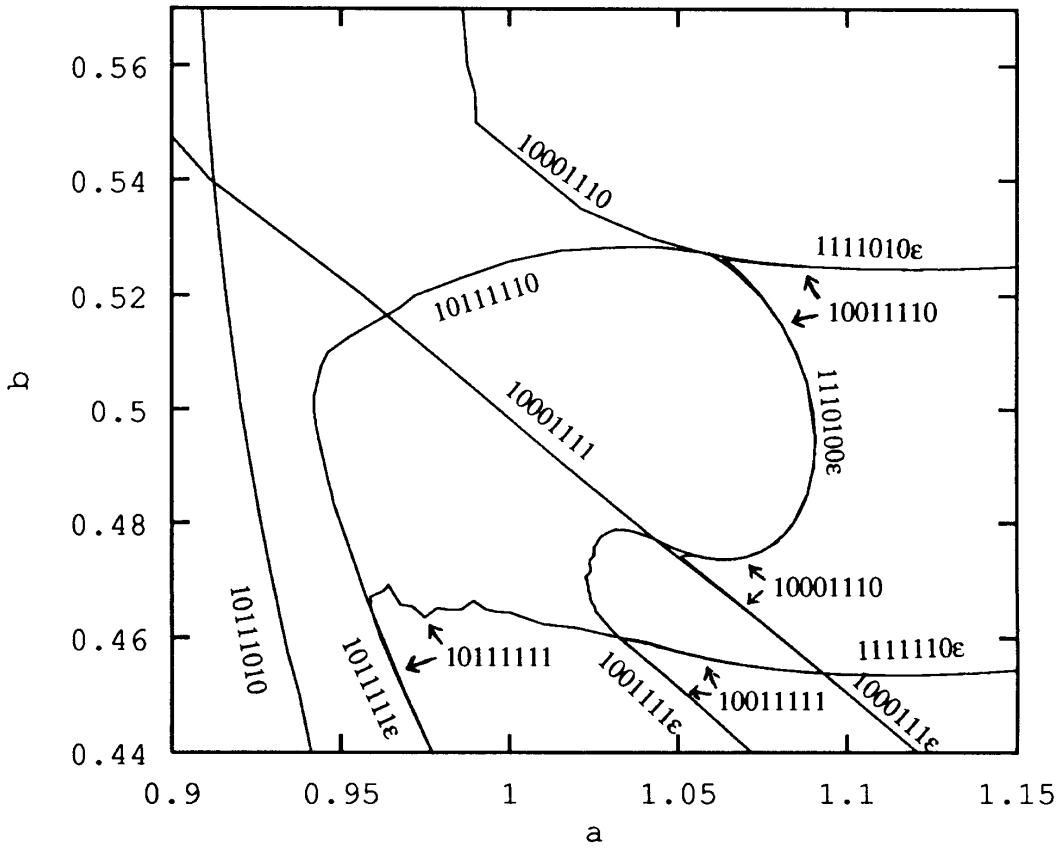

Figure 4.33: The bifurcation of the period 8 orbits in the Hénon map in the parameter space (a, b) calculated with the complex Biham-Wenzel method.

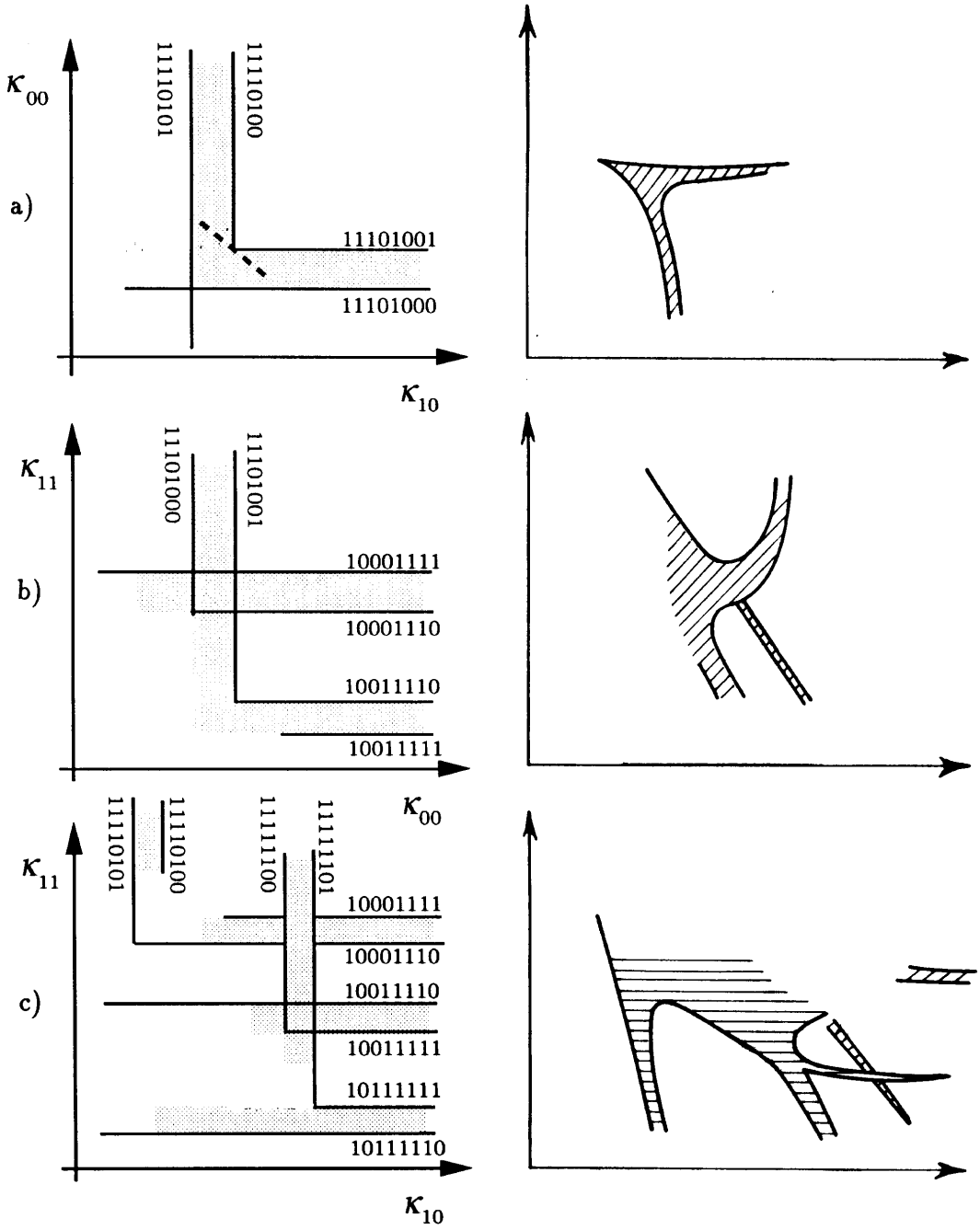

Figure 4.34: The bifurcation lines of some period 8 orbits in the sub-planes of the topological parameter plane and the corresponding structure in the real parameter space. a) $(\kappa_{10}, \kappa_{00})$ b) $(\kappa_{00}, \kappa_{11})$ c) $(\kappa_{10}, \kappa_{11})$

description of the orbit. In figure 4.33 the bifurcation curves are labeled and the double curves that corresponds to a tail are labeled $s_1s_2s_3s_4s_5s_6s_7\epsilon$. This is the cyclic permutation where the two orbits have one different symbol in the end of the string and the two orbits in the tail are pruned on map s_6s_7. All the swallowtail crossings are bifurcations in a two dimensional symbolic parameter plane and in figure 4.34 three pictures show these crosses in three different symbolic parameter planes. Notice that the symbol strings given in the figure have the cyclic rotation giving the largest value $\tau_{s_6s_7}$. If there was a cyclic permutation of an orbit giving a larger $\tau_{s_6s_7}$ then this cyclic permutation would give the correct bifurcation structure.

Figure 4.34 a) shows that the simple cusp of type 2 is a bifurcation in the plane $(\kappa_{10}, \kappa_{00})$ of the three orbits $\overline{11101001}$, $\overline{11101000}$ and $\overline{11110101}$. In agreement with proposition 4 one shift of the symbol string on map 10 with an odd number of 1's give the symbol string on map 00

$$\overline{11101001} = \sigma(\overline{11110100}). \tag{4.47}$$

The figure 4.34 b) shows that the three orbits $\overline{10001111}$, $\overline{10001110}$ and $\overline{11101001}$ bifurcates in a swallowtail crossing in the plane $(\kappa_{00}, \kappa_{11})$. We find that the orbits do not bifurcate along κ_{01} and the bifurcation can therefore not be a cusp where the modality of the map changes.

In figure 4.34 c) we find that the third cross is the bifurcation of the orbits $\overline{10011110}$, $\overline{10011111}$ and $\overline{11111101}$ in the $(\kappa_{10}, \kappa_{11})$ plane. There is no bifurcations giving a cusp and reducing the number of critical point in this plane. From this figure we find that the three tails $\overline{1011111\epsilon}$, $\overline{1001111\epsilon}$ and $\overline{1000111\epsilon}$ bifurcates along the κ_{11} axis and these tails will not cross each other. Figure 4.34 c) also shows that the two tails $\overline{1111010\epsilon}$ and $\overline{1111110\epsilon}$ both bifurcates along κ_{10} and the tails never cross each other.

We find in the (a, b) plane in figure 4.33 the tail $\overline{1111110\epsilon}$ below the tail $\overline{1110100\epsilon}$. In the symbolic parameter plane we do not find that this is necessary as the first tail bifurcates along κ_{10} and the second along κ_{11}.

To further test the symbolic parameter description we numerically investigate the perturbed Hénon map (4.38). The figures 4.35 a) – f) show how the bifurcation structure for the period 8 orbits changes when c changes from $+0.08$ to -0.06. We describe the two extremum cases and some important transitions in the structures.

Figure 4.35 a) for $c = 0.08$ shows that the tail $\overline{1011111\epsilon}$ has become disconnected from the other structure, the cusp of type 2 has not changed while the remaining structure has turned into a bimodal swallowtail crossing and a cusp of type 1. These structures are drawn in the symbolic parameter plane in figure 4.36. In 4.36 a) the two simple cusps are drawn. Both bifurcates in the plane $(\kappa_{10}, \kappa_{00})$ as proposition 4

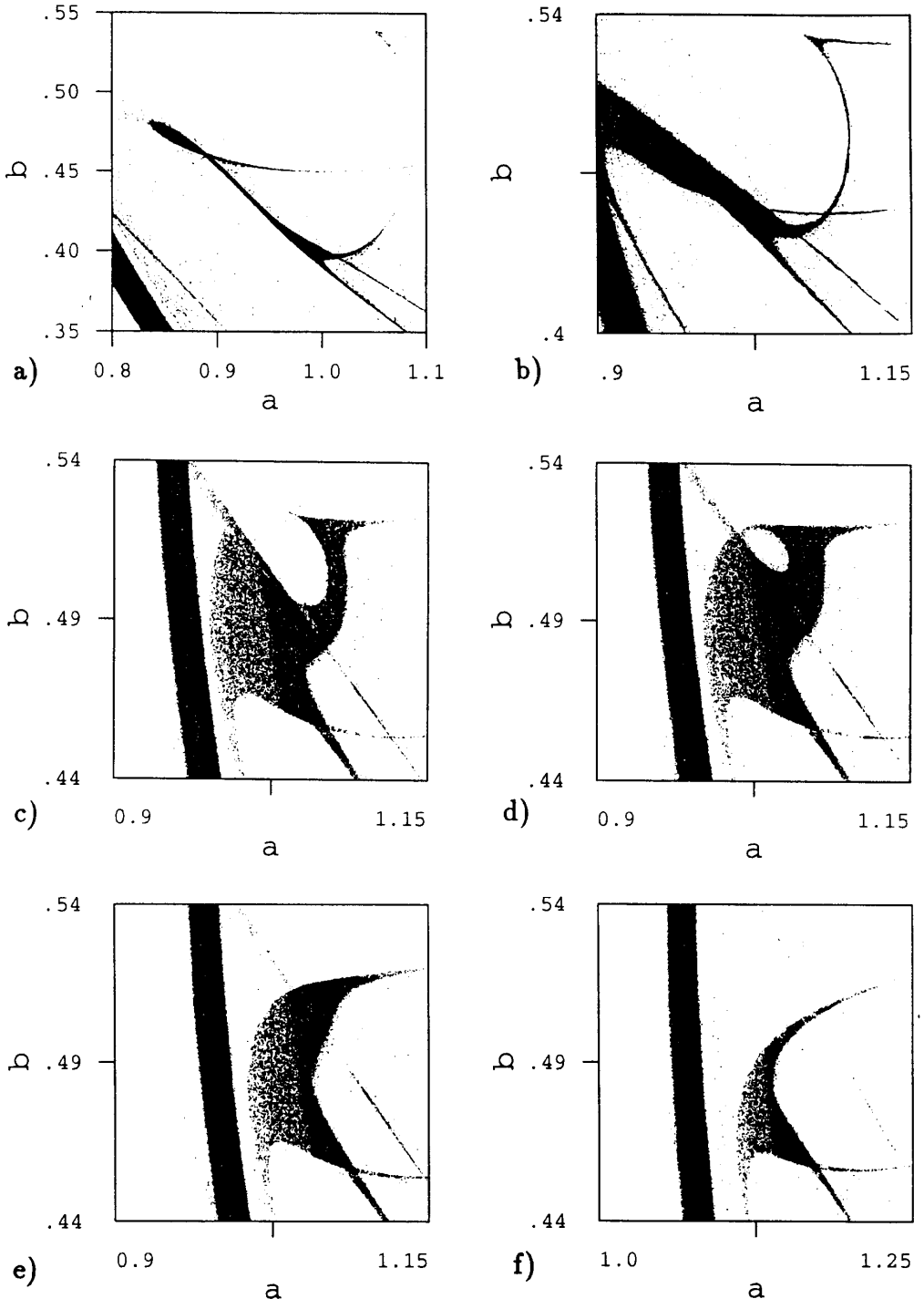

Figure 4.35: The parameter values giving stable period 8 orbits in the perturbed Hénon map (4.38) in the parameter space (a, b) with different values of c. a) $c = 0.08$, b) $c = 0.02$, c) $c = -0.01$ d) $c = -0.013$, e) $c = -0.02$, f) $c = -0.06$.

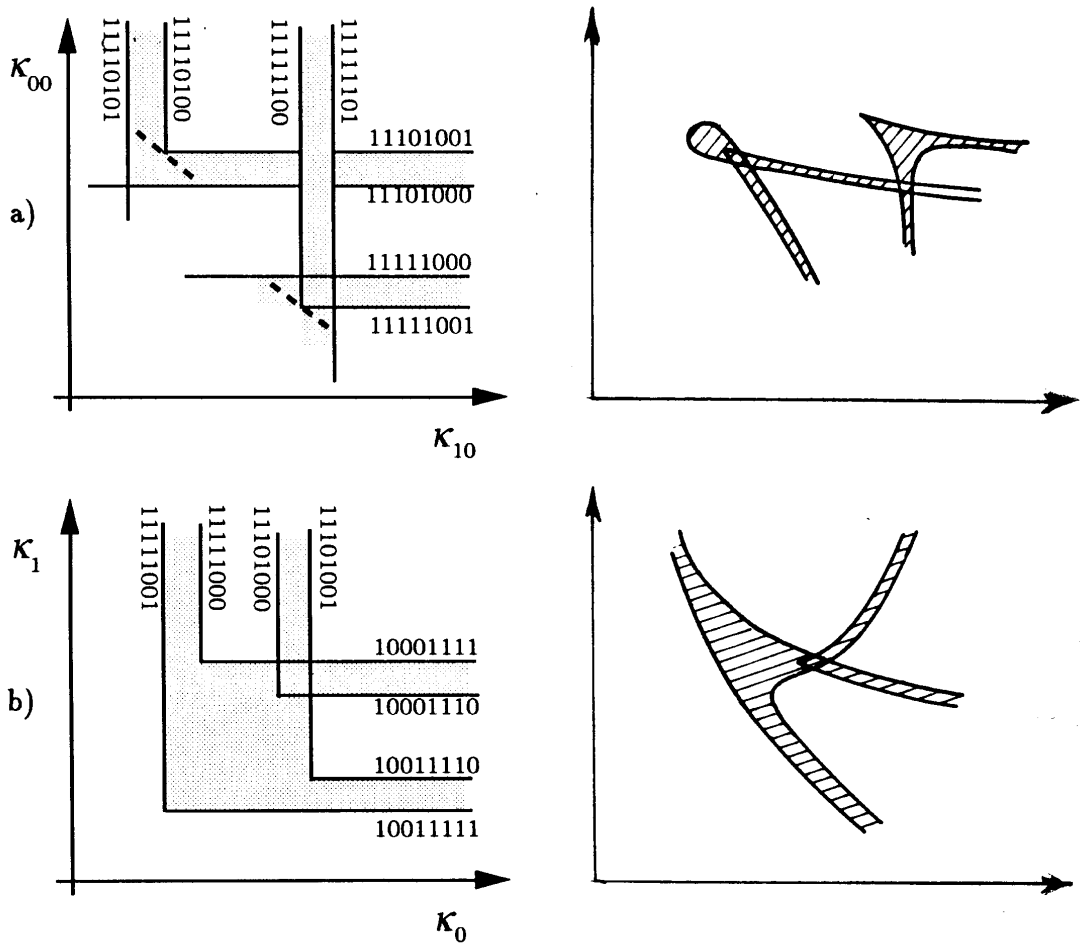

Figure 4.36: Bifurcation lines of some period 8 orbits in the sub-planes of the topological parameter plane and the corresponding structure in the real parameter space for the perturbed Hénon map with $c = 0.08$. a) $(\kappa_{10}, \kappa_{00})$ b) (κ_0, κ_1)

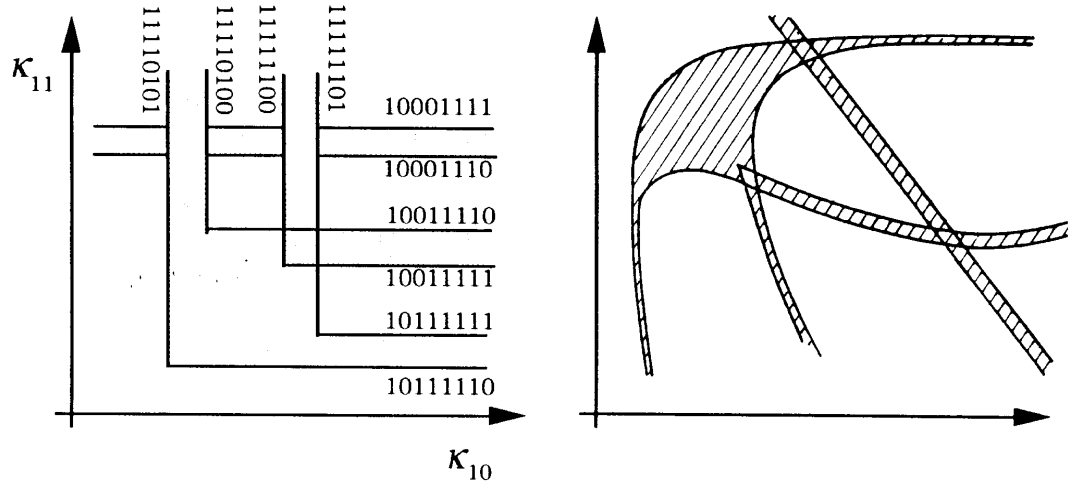

Figure 4.37: Bifurcation lines of some period 8 orbits in the sub-plane $(\kappa_{10}, \kappa_{11})$ of the topological parameter plane and the corresponding structure in the real parameter space for the perturbed Hénon map with $c = -0.06$.

predict. The swallowtail in figure 4.36 b) is one of the bimodal swallowtails in figure 4.19 bifurcating in the bimodal parameter plane (κ_0, κ_1). This example shows that not all the bimodal bifurcation structure can be found in the Hénon map, but when adding new parameters to the map we can find the swallowtails predicted by the bimodal approximation.

We have a different bifurcations structure in figure 4.35 f). For $c = -0.06$ the structure has changed into one simple band and one ordinary swallow tail. This structure is drawn in the topological parameter plane $(\kappa_{11}, \kappa_{10})$ in figure 4.37. The simple band is the tail $\overline{1000111\epsilon}$. The swallowtail looks like the bimodal swallowtails we found in the bimodal approximation but this is not a bimodal structure because the tail $\overline{1111010\epsilon}$ is the cyclic permutation giving $\tau_{10}^{\max}$ but not the cyclic permutation giving $\tau_0^{\max}$. In figure 4.39 we find that the map for $c = -0.06$ indeed is three-folding, but that the period 8 orbit we study here is in the once-folding part of the manifolds.

There is an interesting transition of the bifurcations from figure 4.35 d) ($c = -0.13$) to figure 4.35 e) ($c = -0.2$). In the Hénon map ($c = 0$) there is a tail $\overline{1110100\epsilon}$ connecting two cusp bifurcations. When c decreases this tail merge into a loop and finally disappear. From figure 4.32 it is not easy to guess that this is a possible transition. However from the BW calculations in figure 4.33 we have some bifurcation structures indicating this possibility. A bifurcation line of the orbit $\overline{10111110}$ is going in an arc from the tail $\overline{1011111\epsilon}$ to the tail $\overline{1111010\epsilon}$ exactly as the

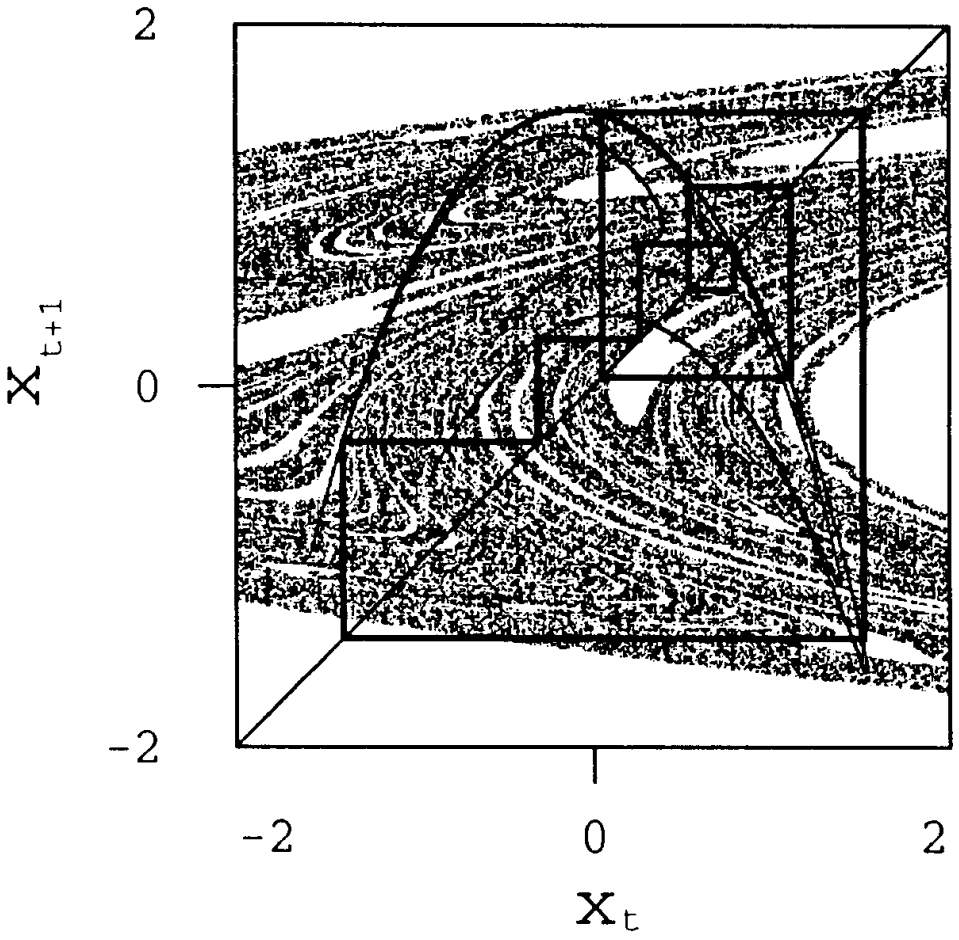

Figure 4.38: The stable period 8 orbit and the manifolds in the cusp in figure 4.35 a) with parameters $a = 0.8683$, $b = 0.4677$, $c = 0.08$.

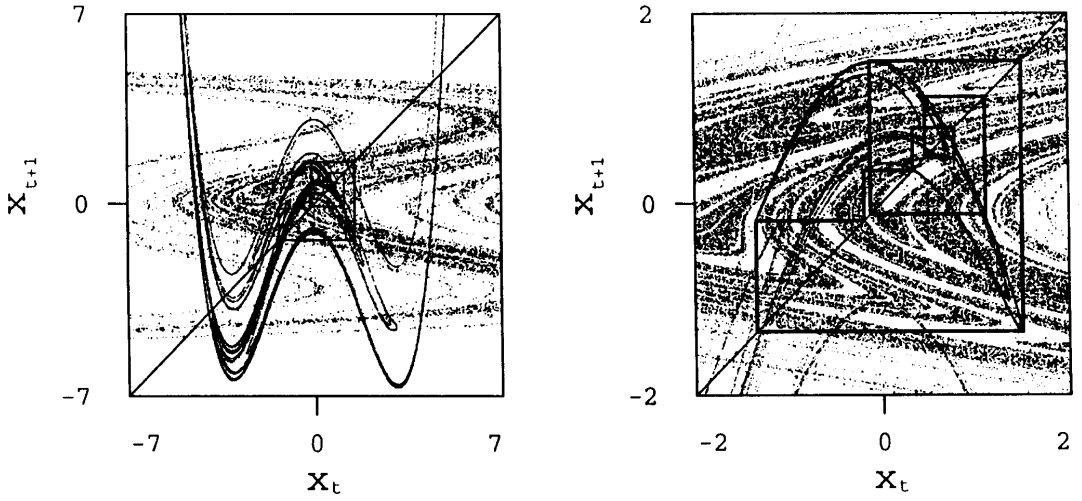

Figure 4.39: The stable period 8 orbit and the manifolds in the swallowtail cross in figure 4.35 f) with parameters $a = 1.15$, $b = 0.465$, $c = -0.06$.

bifurcation line at the back of the swallowtail in figure 4.35 f). In figure 4.32 there is a loop consisting of the tail $\overline{1110100\epsilon}$ and the curves $\overline{10001111}$ and $\overline{10111110}$. If we ignore this loop then we find the following: the four tails $\overline{10\epsilon_1 1111\epsilon_2}$ goes into the bifurcation structure, from down right comes the tail $\overline{1000111\epsilon}$ and to the top left leaves the two curves $\overline{10001110}$ and $\overline{10001111}$. The only difference is that the two orbits $\overline{1000111\epsilon}$ have split up in the left top corner. At the bifurcation point where the loop disappears all three tail $\overline{1000111\epsilon}$, $\overline{1110100\epsilon}$ and $\overline{1111010\epsilon}$ go together at one point and then the stable point is close to the turning-point of the three maps 10, 00 and 11.

4.5 Biham-Wenzel method

After using the method suggested by Biham and Wenzel (BW) to make bifurcations diagrams it is of interest to look closer at this method and its convergence properties.

In earlier investigations [26, 27, 93] this method has been used numerically as a tool to find periodic orbits in the Hénon map. It has been showed by Grassberger et. al [93] that this method fails in certain cases while Biham and Wenzel [27] have replied that that these cases can be solved by introducing some numerical tricks as changing the method slightly or choosing starting points in a special way etc. After the better understanding of symbolic dynamics given here and the study of the convergence of the BW method as a function of the (a, b) plane is it useful to discuss the method again. The motivation of Biham and Wenzel was a Hamiltonian

formalism, but we find this irrelevant and we will not discuss this argument.

Biham and Wenzel have suggested one method finding only real solutions and a more complicated method which also finds complex solutions for a (possibly) complex Hénon map. Biham and Wenzel uses the convention of the Hénon map

$$x_{t+1} = a - x_t^2 + bx_{t-1} \tag{4.48}$$

which is turned into the map we use by changing $x \to x/a$ while the parameters a and b are the same.

The real BW method to find a period n orbit works as follows [26]: Choose x_i for $i \in \{1, 2, \ldots, n\}$ to be random numbers and let $x_0 = x_n$ and $x_{n+1} = x_0$. Let then the values x_i evolve with time according to the differential equation

$$\dot{x}_i = s_i F_i, \qquad i = 1, \ldots, n \tag{4.49}$$

with

$$s_i \in \{-1, 1\}$$

and

$$F_i = -x_{i+1} + a - x_i^2 + bx_{i-1} \tag{4.50}$$

The "force" F_i is just a rewriting of the Hénon map (4.48) which is equal 0 if the values x_i are the points in a period n orbit of the Hénon map. The periodic orbits we are interested in are one possible solution of eq. (4.49) and it is not very surprising that this kind of method may work. What is interesting is that the choice of values s_i gives a symbolic dynamics and that this symbolic dynamics with $s = -1 \to s = 0$ in most cases is the same symbolic dynamics as the Smale horseshoe type of symbols.

Biham and Wenzel also have extended this method to a complex version which can include complex parameters and gives the complex periodic orbits when the real orbits do not exist [27]. By using real parameters this method gives the real and the imaginary solutions of periodic orbit if the method converges. The advantage with this method is that we can check whether we did not get the real periodic orbit because the orbit was imaginary or because the method failed to converge.

Let all the variables in the equations above become complex numbers with $z_i = x_i + iy_i$ where $z_0 = z_n$ and $z_{n+1} = z_0$, and $F_i = f_i + i\phi_i$, $A = a + i\alpha$ and $B = b + i\beta$. The differential equation we choose as before to be

$$\dot{z}_i = c_i F_i, \qquad i = 1, \ldots, n \tag{4.51}$$

with

$$F_i = -z_{i+1} + A - z_i^2 + Bz_{i-1} \tag{4.52}$$

but here we choose

$$c_i = s_i + i\,\mathrm{sgn}(y_i)$$

with $s_i \in \{-1, 1\}$ the symbols as in the real case. The introduction of the $i\,\mathrm{sgn}(y_i)$ terms seems to be just ad hoc but numerical experiments show that this term is necessary to get a convergence to the complex solutions.

Writing the differential equations as two real equations give

$$\begin{aligned} \dot{x_i} &= s_i\left(-x_{i+1} + a - x_i^2 + y_i^2 + bx_{i-1} - \beta y_{i-1}\right) \\ &\quad +\mathrm{sgn}(y_i)\left(-y_{i+1} + \alpha - 2x_i y_i + \beta x_{i-1} + by_{i-1}\right) \end{aligned} \tag{4.53}$$

and

$$\begin{aligned} \dot{y_i} &= s_i\left(-y_{i+1} + \alpha - 2x_i y_i + \beta x_{i-1} + by_{i-1}\right) \\ &\quad +\mathrm{sgn}(y_i)\left(-x_{i+1} + a - x_i^2 + y_i^2 + bx_{i-1} - \beta y_{i-1}\right) \end{aligned} \tag{4.54}$$

These equations with $\alpha = \beta = 0$ have we used to find the bifurcation lines in the parameter space integrated with a fourth-order Runge-Kutta method.

Figure 4.7 shows that for the short orbits of length 1, 2 and 3 the bifurcation lines the BW method gives is the same lines as the bifurcation lines where these orbits start to exist.

In the swallowtail in figure 4.11 the BW does not converge to the stable orbit in the center of the cross. In this region the stable orbit in a one dimensional bimodal map changes symbolic dynamics in a complicated way. The BW method solves this problem of choosing the right symbolic description by not converging at all.

More interesting is the bifurcation curves close to the simple cusp as in figure 4.26. On the back of the cusp the BW does not converge to the unstable orbit. It is natural to relate this to the change of modality on the back side of the cusp. As one adiabatically changes the parameters and follows the unstable orbit one observe that the orbit start with one symbolic description and then has to change to an other symbolic description. In the area where there is a smaller modality of the map there is no obvious reason why one or the other of the symbol string should make the BW converge. Assume that the BW artificial dynamics makes the points move in one direction away from the turning point and the direction is determined by the symbol, then it is a reasonable guess that it does not converge when the turning point vanishes.

The numeric indicate that that the BW method in this case converges for parts of the parameter space where the map has lost its turning point. In figure 4.40 the curves where BW losses convergence for the period 6 and 8 orbits are drawn together with the dashed curve where the fold ...101111 looses its turning point.

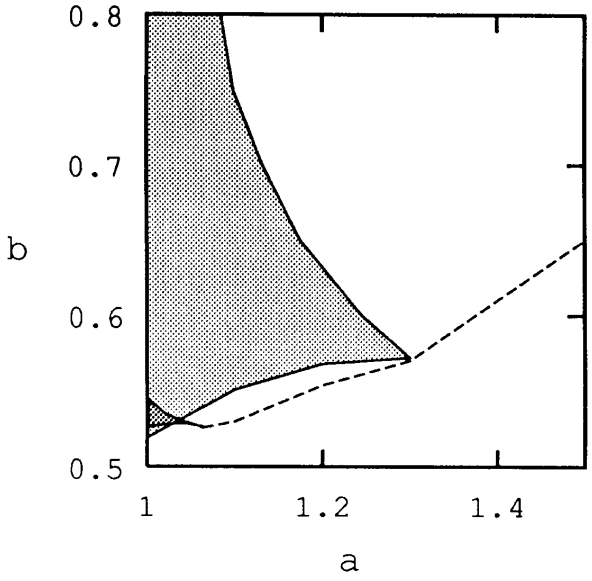

Figure 4.40: Border curves where the complex Biham-Wenzel method fails to converge for period 6 and 8 orbits. The dashed curve is the bifurcation line where the fold ...101111 looses its turning point.

This dashed curve is obtained simply by looking at pictures of the stable and the unstable manifold and judge by eye if the fold has a primary turning point or not. When the parameters get closer to the lines where the BW method fails, then the convergence of the BW method gets slower and slower. In the area where it fails to converge it also fails if we starts close to the correct solution. The periodic orbit can be found by a Newton algorithm and followed adiabatically through the parameter plane where it exists as done in ref. [107].

In ref [27] Biham and Wenzel discuss the convergence of the period 8 orbit $\overline{10001110}$ for parameters $a = 1.0$ and $b = 0.54$. They find that the method converges to a limit circle and not to a periodic orbit but that when one multiply the left side of eq. (4.54) with a number larger than 1.43 such that the x and y values do not converge with the same speed then the method converges to the right solution. They use this example as an argument that the method will converge with small adjustments.

We have in figure 4.33 plotted the curve where the method does not converge any more for the orbit $\overline{10001110}$. For the parameter $b = 0.54$ we find the bifurcation line at $a = 1.0105$ which imply that the method does not converge to the orbit for $a = 1.0$ but this parameter is very close to the convergence region. These parameters are above a cusp in figure 4.32. We correctly find that by increasing the relative size

of eq. (4.54) compared to eq. (4.53) we obtain a converging method for $a = 1.0$. The value of a where the method stops converging decreases but it reach a minimum value at approximately $a = 0.985$ when we choose (4.54) to be around 8 times as large as (4.53) and then a increases again for larger ratios. This numerical trick seems to be able to move the bifurcation line slightly, but not enough to prevent that in a large area the method fails to converge.

The dashed line in figure 4.40 represents the most important of the bifurcations reducing the modality of the map. There are similar lines arbitraryly close to the $b = 0$ line and therefore we conjecture that for any parameter value of the pruned Hénon map, the BW method will fail to find all periodic orbits existing. The orbits it fails to find are those which are above a cusp bifurcation and therefore do not have a unique symbolic description even in a one dimensional map.

4.6 Twice-folding maps

The twice-folding horseshoe map has parameter space of higher dimension than the once-folding map and a bifurcation structure that is more difficult to draw in a symbolic parameter space. We will only discuss a few examples of bifurcations and show that that these are consistent with the symbolic parameter space description.

The map we choose for illustrating the twice-folding bifurcations is

$$x_{t+1} = x_t^3 - ax_t + b + Bx_{t-1} \tag{4.55}$$

Instead of adding a cubic term to the Hénon map we choose to use the cubic map in section 2.1 and add a term Bx_{t-1} to this. As for the Hénon map this map reduces to a one dimensional map for $B \to 0$ and the bifurcations of the map $B = 0$ is discussed in section 2.1. The bifurcations we find in section 2.1 can be considered a first order approximation valid for small values of B and some of these bifurcations are shown in figures 2.4, 2.6 and 2.8. This is bifurcations in a two dimensional parameter space.

The second approximation gives three bimodal maps with the topological parameters given by the 6 kneading values of the 6 independent extremum points in the approximation. The ordering of the kneading values depends only on the sign of B. As for the Hénon map we find that for $B > 0$ the horseshoe is orientation reversing and

$$\kappa^1_{\text{map }0} < \kappa^1_{\text{map }1} < \kappa^1_{\text{map }2} \tag{4.56}$$

$$\kappa^2_{\text{map }0} < \kappa^2_{\text{map }1} < \kappa^2_{\text{map }2} \tag{4.57}$$

For the orientation preserving case $B < 0$ we have

$$\kappa^1_{\text{map } 2} < \kappa^1_{\text{map } 1} < \kappa^1_{\text{map } 0} \tag{4.58}$$

$$\kappa^2_{\text{map } 2} < \kappa^2_{\text{map } 1} < \kappa^2_{\text{map } 0} \tag{4.59}$$

One interesting new bifurcation structure is the bifurcations of the period 3 orbits. In the parameter space (a, B) for $b = 0$ we find that the two tails $\overline{22\{0,1\}}$ and $\overline{21\{0,1\}}$ cross each other when B increases and that the tail $\overline{21\{0,1\}}$ has a cusp bifurcation of type 2 (see page 127) shown in figure 4.41. The stable orbit in the cusp is drawn in figure 4.42 together with the stable and the unstable manifolds, and the stable orbit in the other tail in figure 4.41 is drawn in figure 4.43 together with the unstable manifold.

The cusp has the two tails $\overline{21\{0,1\}}$ and $\overline{02\{1,2\}}$, where the stable orbit $\overline{210}$ is the common orbit. This kind of structure is familiar from the Hénon map parameter spaces. We can find the bifurcation diagram in a universal two dimensional symbolic symbol plane drawn in figure 4.44 a). This is the bifurcation plane with the two symbolic parameters $\kappa^1_{\text{map } 1}$ and $\kappa^2_{\text{map } 2}$. The symbolic parameter subspace $(\kappa^1_{\text{map } 1}, \kappa^2_{\text{map } 2})$ has the structure in figure 4.44 when all other values of κ is constant and when $\kappa^1_{\text{map } 2}$ is sufficiently large; $1 \geq \kappa^1_{\text{map } 2} >> \kappa^1_{\text{map } 1}$ As for the once-folding map, the common orbit is in this case related in the two tails by a single shift of symbols. A generalization of proposition 4 to the twice-folded map is straight forward.

The first order approximation predicts that these two orbits bifurcate in an ordinary swallowtail bifurcation. This bifurcation is showed in the ordinary parameter space and the topological parameter space in figures 2.6 and 2.7. We can numerically study the transition from this swallowtail to the isolated cusp in figure 4.44 by following the bifurcations in the (a, b) plane as B increases.

At $B = 0.12$ figure 4.45 shows that the two tails $\overline{21\{0,1\}}$ and $\overline{22\{0,1\}}$ are closer in the parameter space, but topologically there is still a connected swallowtail with the tails ordered as for $B = 0$. At $B = 0.2$, figure 4.46, the two tails have changed order, such that $\overline{22\{0,1\}}$ is to the left of $\overline{21\{0,1\}}$ and the crossing is broken up into one cusp and one tail. This tail is thicker close to the cusp because there the unstable manifold bends less sharp here.

The sketch of bifurcation lines in figure 4.44 b) is drawn as expected from a Biham-Wenzel type algorithm. In the area above the cusp the unstable period 3 orbit has to change its symbolic description and it does not have a definite description in a 3 letter alphabet. We expect that if we could construct an algorithm of this type it would fail to converge in this area.

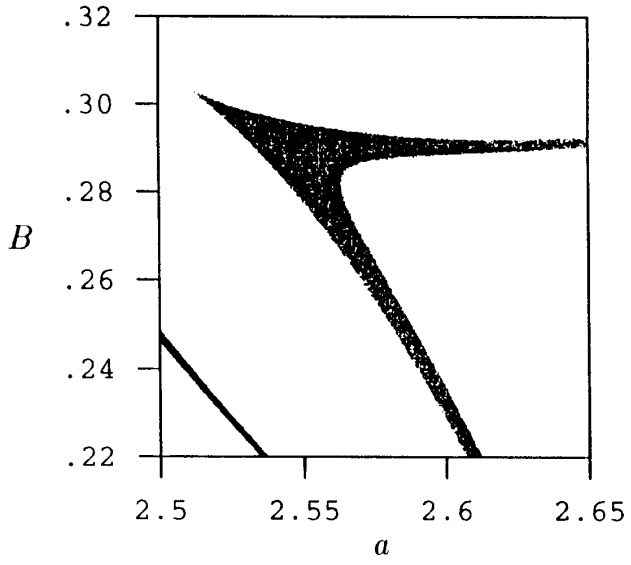

Figure 4.41: The area in parameter space (a, B) of the twice-folding map $b = 0$ where period 3 orbits are stable.

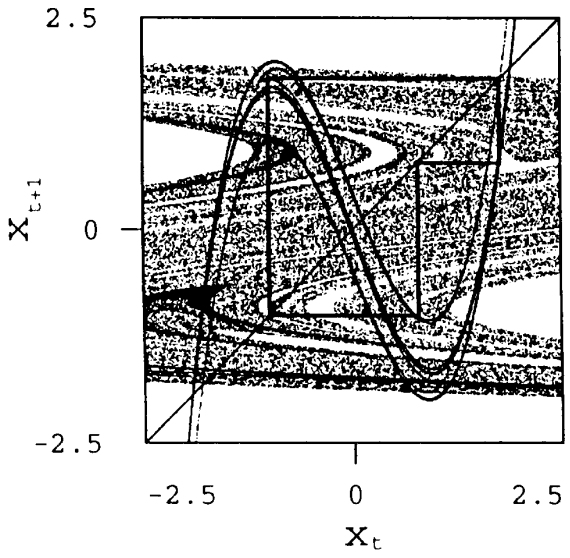

Figure 4.42: The stable and the unstable manifolds and the stable period 3 orbit $\overline{210}$ in the cusp bifurcation $a = 2.55$, $b = 0$, $B = 0.29$.

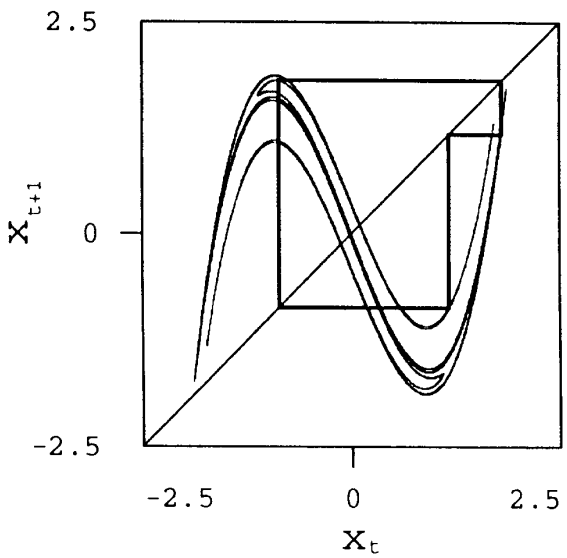

Figure 4.43: The unstable manifold and the stable period 3 orbit $\overline{221}$ $a = 2.5$, $b = 0$, $B = 0.2485$.

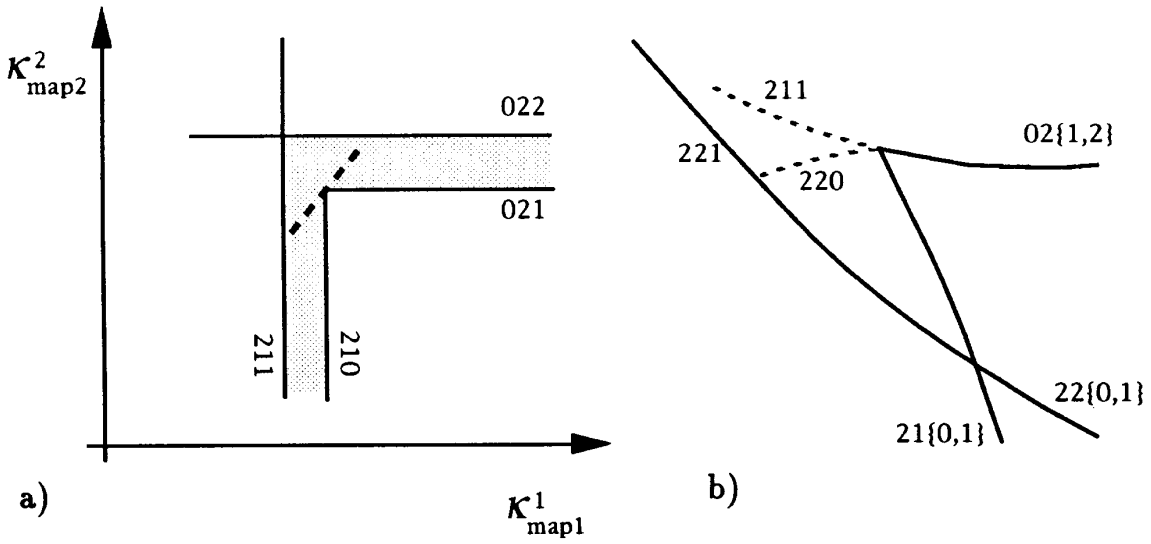

Figure 4.44: a) Bifurcation lines for period 3 orbits in a two dimensional subspace $(\kappa^1_{\text{map }1}, \kappa^2_{\text{map }2})$ of the symbolic parameter space of the twice-folding map. b) A sketch of bifurcation lines in the parameter space (a, B).

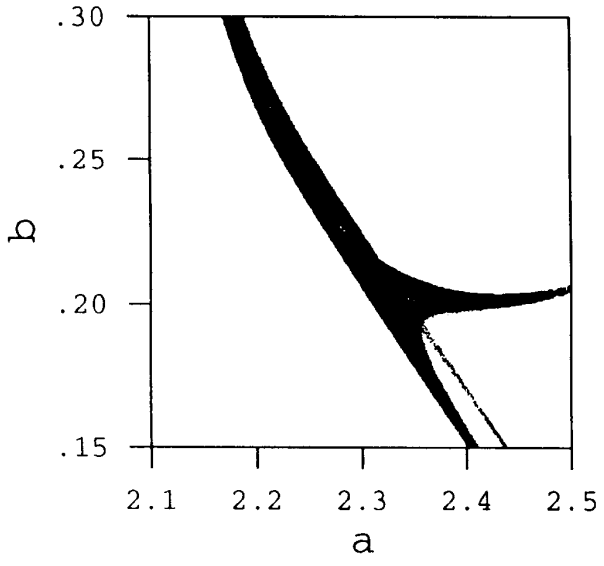

Figure 4.45: The area in parameter space (a, b) of the twice-folding map $B = 0.12$ where period 3 orbits are stable.

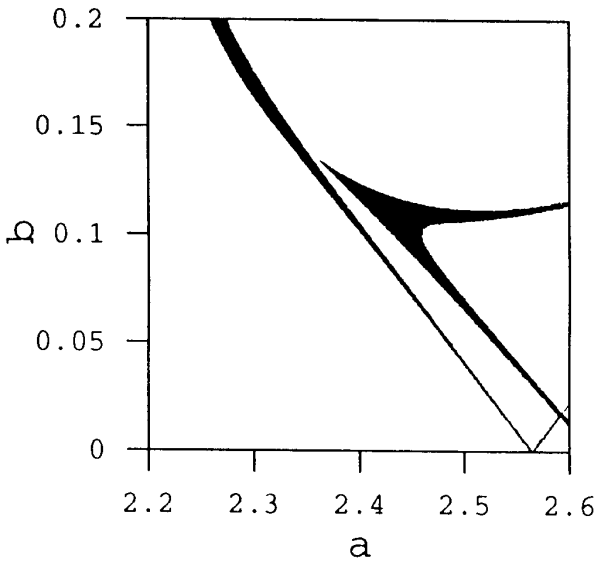

Figure 4.46: The area in parameter space (a, b) of the twice-folding map $B = 0.2$ where period 3 orbits are stable.

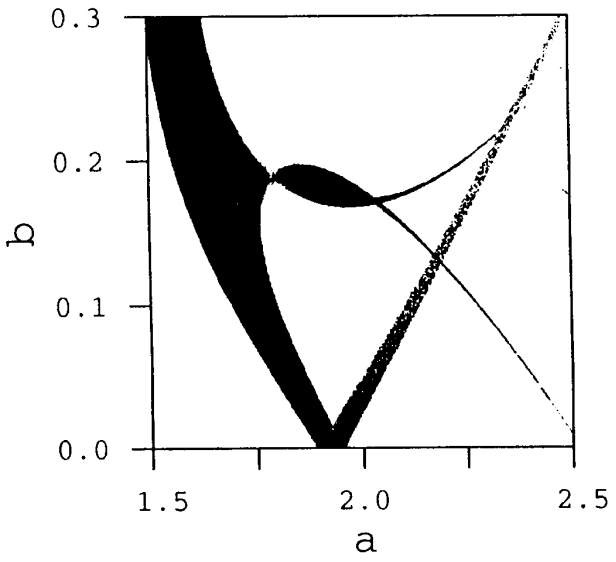

Figure 4.47: The area in parameter space (a, b) of the twice-folding map $B = 0.2$ where period 4 orbits are stable.

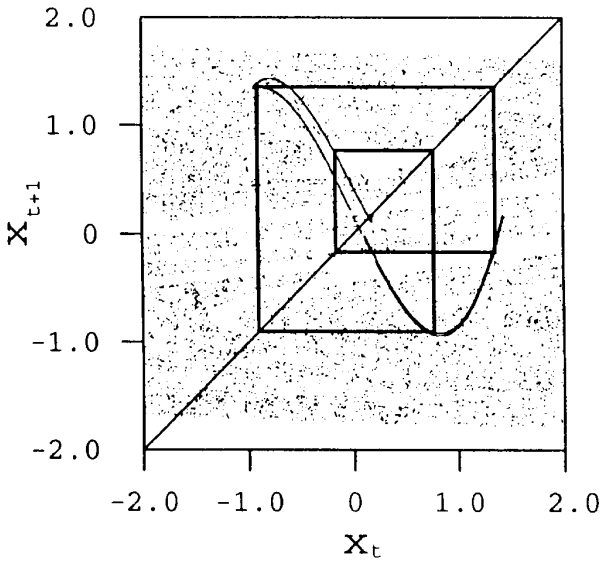

Figure 4.48: The unstable manifold and the stable period 4 orbit in the cusp of figure 4.47 $a = 1.95$, $b = 0.175$, $B = 0.2$.

A different example of the breakup of the swallowtail is given by the period 4 orbit swallowtail cross $\overline{21\{1,2\},\{0,1\}}$. In the $B = 0$ limit this is an ordinary swallow tail shown in figure 2.8. When B increases, this tail splits up, but in a different way than in the period 3 example above. In this case the inner part of the crossing becomes disconnected, and we get a cusp bifurcation of the type where the unstable orbit is the common orbit in the two tails. This does not require crossing of tails; figure 4.47 shows the bifurcation structure in the plane (a, b) for $B = 0.2$. The manifolds and the stable orbit in the isolated cusp are drawn in figure 4.48. The cusp is isolated if the symbolic value $\kappa^1_{\text{map }2}$ is sufficiently larger than $\kappa^1_{\text{map }1}$ which in ordinary parameters means that B is sufficiently large. The symbolic parameter plane $(\kappa^1_{\text{map }1}, \kappa^2_{\text{map1}})$ gives this cusp bifurcation with the two tails $\overline{211\{0,1\}}$ and $\overline{021\{1,2\}}$.

The structures we find numerically for this model all fits into the description with a symbolic parameter space organized hierarchically with approximations with 2 parameters, 6 parameters, 18 parameters, etc. We conjecture that the symbolic parameter space describes all bifurcations in this map.